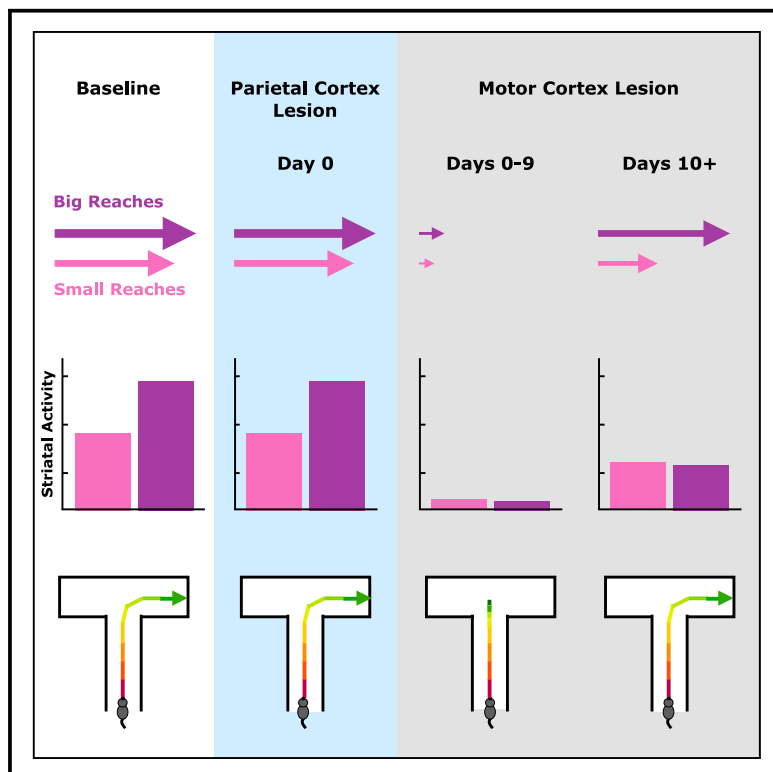


Motor cortex is responsible for motoric dynamics in striatum and the execution of both skilled and unskilled actions

Graphical abstract



Authors

Mark A. Nicholas, Eric A. Yttri

Correspondence

mnichola@andrew.cmu.edu (M.A.N.),
eyttri@andrew.cmu.edu (E.A.Y.)

In brief

Nicholas and Yttri find that in the absence of motor cortex, the striatum alone is not capable of producing goal-directed behavior. Lesions of motor cortex also produce a freezing of gait-like behavior, implicating motor cortex in the setting and updating of motor state.

Highlights

- Motor, but not parietal, cortex is necessary for performing goal-directed actions
- Movement-related dynamics in the striatum are absent following lesions of M1
- Behavior and striatal activity partly recover but are not comparable to pre-lesion
- M1 lesions cause freezing of gait, suggesting its role in motor-state regulation

Article

Motor cortex is responsible for motoric dynamics in striatum and the execution of both skilled and unskilled actions

Mark A. Nicholas^{1,2,*} and Eric A. Yttri^{1,2,3,4,*}

¹Department of Biological Sciences, Carnegie Mellon University, Pittsburgh, PA 15213, USA

²Center for the Neural Basis of Cognition, Carnegie Mellon University and University of Pittsburgh, Pittsburgh, PA 15213, USA

³Neuroscience Institute, Carnegie Mellon University, Pittsburgh, PA 15213, USA

⁴Lead contact

*Correspondence: mnichola@andrew.cmu.edu (M.A.N.), eyttri@andrew.cmu.edu (E.A.Y.)

<https://doi.org/10.1016/j.neuron.2024.07.022>

SUMMARY

Striatum and its predominant input, motor cortex, are responsible for the selection and performance of purposive movement, but how their interaction guides these processes is not understood. To establish its neural and behavioral contributions, we bilaterally lesioned motor cortex and recorded striatal activity and reaching performance daily, capturing the lesion's direct ramifications within hours of the intervention. We observed reaching impairment and an absence of striatal motoric activity following lesion of motor cortex, but not parietal cortex control lesions. Although some aspects of performance began to recover after 8–10 days, striatal projection and interneuronal dynamics did not—eventually entering a non-motor encoding state that aligned with persisting kinematic control deficits. Lesioned mice also exhibited a profound inability to switch motor plans while locomoting, reminiscent of clinical freezing of gait (FOG). Our results demonstrate the necessity of motor cortex in generating trained and untrained actions as well as striatal motoric dynamics.

INTRODUCTION

Even the simplest of actions, such as reaching or orienting, requires the coordinated interaction of several brain regions. Primary motor cortex (M1) demonstrates complex dynamics^{1,2} and is widely thought to generate motor commands, although the specific values encoded to support this function are unclear.^{3–9} Causal manipulations have provided additional insights into its functional contribution. M1 stimulation induces actions of varying complexity, consistent with a role in the generation of action plans,^{5,10–12} while lesions and inactivation produce an array of motor deficits.^{13–16} Temporally and anatomically precise photoinactivation of M1 has been shown to prevent action initiation in the upcoming or evolving movement.^{17,18} These effects are specific to skilled motor actions while sparing more naturalistic behaviors.^{18,19} This same targeted method has been used to demonstrate the necessity of M1 for selecting between actions.²⁰ However, recent lesion studies using ibotenic acid and physical aspiration lesions found no effect on learned, non-dexterous task performance in rats.²¹ In a similar study, inactivation of mouse M1 did not impair behavior after extensive learning in a cued joystick-based forelimb reaching task.²² These studies cast doubt on previous models of M1 function and have brought into question the extent to which the rodent and primate M1 fulfill fundamentally different computational needs.²³

Instead of M1 driving the generation of actions to be performed, the basal ganglia has been suggested to be the seat of selection and execution of actions.²⁴ Electrical stimulation of the caudate or inactivation of the substantia nigra elicits contralateral saccades.²⁵ In a groundbreaking study, it was shown that several seconds of continuous optogenetic stimulation was sufficient to induce or suppress locomotion, depending on the striatal projection population being stimulated.²⁶ Related work incorporating action value has demonstrated that stimulation can induce the performance of one action over another. Selective stimulation of either striatal projection pathway biased the selection of movements to a left or right reward port.²⁷ Recently, a series of lesion studies found evidence suggesting that the dorsal striatum may be responsible for the generation of skilled movements.^{21,28} Notably, it was suggested that thalamic inputs, not motor cortical inputs, support the basal ganglia in this function. This stands in sharp contrast to other models in which M1 generates the motor command to be executed while the basal ganglia modulates its kinematic performance^{29,30} via reentrant projections to subcortical motor centers where cortical and basal ganglia information converges.³¹ This interpretation of cortico-basal ganglia function was originally based on the pathological hypo- or hyperkinesia that defines disorders affecting the basal ganglia, like Parkinson's and Huntington's diseases,^{32–34} and has empirical support. Selective stimulation of striatal

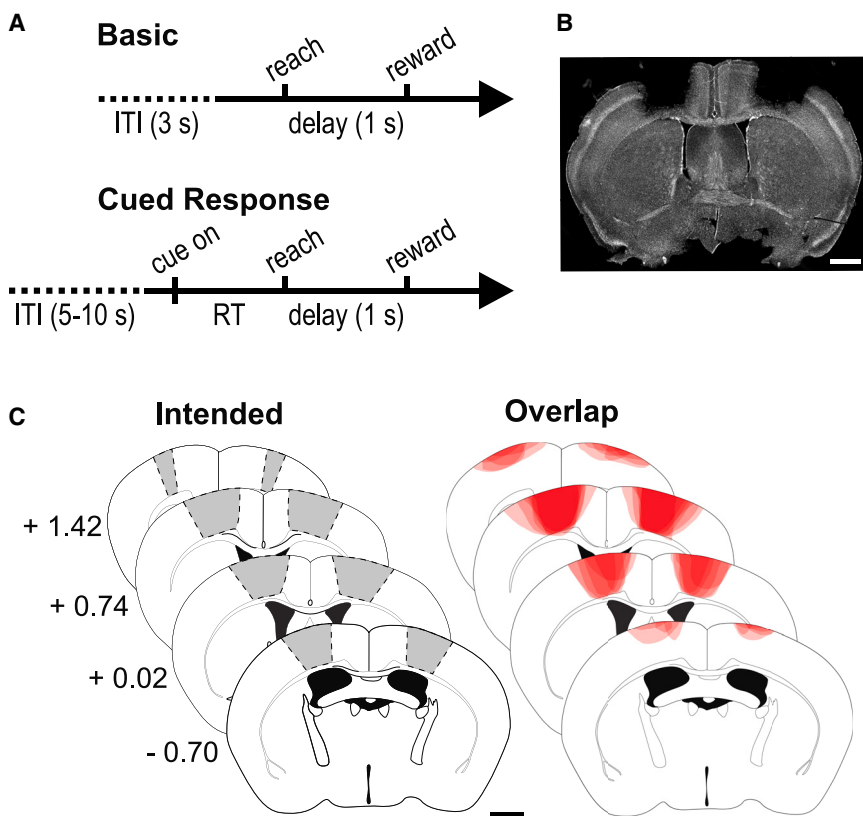


Figure 1. Task design and lesion quantification

(A) Mice were trained to perform a basic uncued or cued forelimb reaching task.

(B) Example bilateral M1 aspiration lesion, 0.25 mm anterior to bregma. Scale bar depicts 1 mm.

(C) Reconstruction of bilateral M1 lesions. Left: coronal sections from a standard mouse brain depicting the extent of the caudal forelimb area. Numeric values depict distance from bregma in mm. Right: extent and overlap of the lesions from the 8 mice used in the basic uncued and cued response tasks. Scale bar depicts 1 mm.

revealing how compensatory supportive processes arise over time.

Given this information, we sought to understand the contribution of M1 to striatal and behavioral dynamics. Following lesions of M1, mice were unable to perform either the self-paced or cued movement tasks. However, many aspects of behavior “recovered,” starting around day 10 post lesion. The presence of a go cue did not mitigate the effects nor timing of recovery. Critically, movement-related dynamics that are normally prevalent in the spiny projection neurons (SPNs) and fast-spiking interneurons (FSIs) of the striatum were absent in the

projection populations,³⁵ or elimination of basal ganglia output,^{36,37} induces small kinematic changes rather than pronounced action selection or initiation deficits. However, it may be difficult to disentangle the motor contributions of M1 and its major target, the dorsal striatum. The motor cortex projection constitutes a major input to the striatum, with a wide array of cell types coming from both superficial and deep layers of M1 sending monosynaptic projections to the striatum.^{38–41} Not surprisingly, these areas also demonstrate coupled dynamics. Phase-coupling between the areas occurs during both rewarded and unrewarded actions, and the coherence of these dynamics is correlated with action speed.^{42,43}

Given this, a broader circuit approach may be beneficial to understand whether and how corticostriatal dynamics underlie movement. We sought to identify the contribution of M1 to both behavior and concurrent striatal dynamics. Cohorts of mice were trained to perform either a self-paced or cued center-out movement task. We recorded dorsal striatal and behavioral dynamics in daily sessions, then bilaterally lesioned the caudal forelimb area (CFA) of M1 while continuing neurobehavioral monitoring in the task—including on the day of lesion. Pairing the immediate effects of causal lesions with correlative recordings provided the means to determine what information from the complex cortical dynamics is conveyed through to striatum⁴⁴ and how these areas fit into the broader orchestration of motor control nodes.⁴⁵ Unlike more targeted methods such as photo-inactivation, lesioning affects all of the cell types and layers of motor cortex that serve as inputs to the striatum,⁴⁶ while also

days following the lesion in those movements that did occur. Performance greatly improved by post-lesion day 10 and striatal responses were observed; however, this activity was no longer tied to kinematic dynamics and its presence lagged behind the behavioral improvement. Comparably sized lesions of the sensorimotor parietal cortex had no such effects. In light of these results, we raised the question as to whether these effects were limited to learned skilled motor actions. To establish the contribution of M1 to movement outside of a trained task, we allowed mice to explore an unrewarded T-maze and observed that while lesioned mice could locomote, the ability to select a new motor state, e.g., switching from locomotion to turning at the threshold of the T-maze hallways, was grossly impaired.

RESULTS

To empirically assess theoretical models concerning the contribution of M1 to both behavior and striatal dynamics, we bilaterally aspirated CFA of M1 in mice that had learned either a self-paced or a cued movement task (Figure 1; Video S1). Lesions provide an interventional state that extends across all task epochs, as well as the ability to identify and dissociate the immediate and compensatory effects of the intervention.^{47,48} It has also been suggested that the results of transient manipulations overstate the actual neural contributions.⁴⁹ More importantly, in addition to the well-known glutamatergic projections arising from intratelencephalic and pyramidal tract neurons spanning

different layers of the cortex, M1 also sends both somatostatin- and parvalbumin-positive GABAergic projections to the dorsal striatum.⁴⁶ As such, cell-type-specific manipulations are incomplete interventions. Aspiration lesions of M1 have previously been shown to induce the same effects as pharmacological lesions (e.g., ibotenic acid).²¹ To preclude the inclusion of potential compensatory mechanisms surrounding the manipulation,^{48,50–53} behavior and striatal activity were recorded 3.5 h after the animal had fully recovered⁵⁴ from surgical anesthesia and in once-a-day sessions every day following. As a control for the general effects of lesion, a separate cohort received lesions of approximately the same volume of tissue, bilaterally centered in the posterior parietal cortex (PPC), the null results of which are discussed later in the manuscript.

CFA is required for the performance of learned movements

Mice either learned a center-out or cued task requiring displacement of a joystick (a “reach”) at least 0.9 cm in any direction using both arms (Figure 1A⁵⁵). Throughout pre- and post-lesion sessions, the forepaws typically remained on the joystick, gripping the horizontal bar. After several weeks of training, animals readily performed self-paced, uncued reaches with a consistent inter-reach interval, amplitude, peak speed, trajectory, and duration (Figure 2). For concision, sessions were assigned to a 5-day epoch relative to the day of lesion: Pre (1 to 5 days before lesion), Post 1 (0–4 days after lesion), Post 2 (5–9 days after lesion), and so forth.

In pre-lesion sessions, mice performed on average 9.0 ± 0.73 (mean \pm SEM) rewarded reaches per minute over the first 20 min of each session. Following lesion of M1, however, mice were mostly unable to perform the reaching task. In the 5 days following bilateral M1 lesions (Post 1), performance was reduced to 0.23 ± 0.07 (mean \pm SEM) rewarded reaches per minute (Figure 2A). The ability to execute reaches improved around days 8–10, but the trial rate did not recover to pre-lesion levels within the nearly 3 weeks of post-lesion monitoring (Figure 2A, $P < 0.008$, two-sample t test; all multiple comparisons are Bonferroni corrected unless noted otherwise). Although aspects of this later recovery may be informative in understanding compensatory mechanisms, we stress that the assessment of lesion effect is most accurate in the days immediately following the manipulation.

In the days following the lesion, those forelimb movements that did occur were severely impaired. Given the relative inability to execute movements of a sufficient amplitude to receive a reward, we characterized the performance of any joystick movement greater than 0.05 cm. The inter-reach interval for all detected movements only returned to baseline in Post 4 (Figure 2B, Pre vs. Post 1–3, $P < 0.04$, Pre vs. Post 4, uncorrected $p = 0.48$; cumulative histograms show performance of individual reaches, although all statistics reflect per-session averages). Of those movements that did occur, most were quite small, with a median amplitude of 0.22 cm across all movements in either Post 1 or Post 2 epochs (for comparison, Figure 2C, Pre median amplitude was 1.54 cm). Movements of such small amplitude accounted for only 3.8% of the pre-lesion performance. Over successive days, and commensurate with the jump in rewarded perfor-

mance around day 9, we observed the development of a bimodal distribution consisting of the low-amplitude (under 0.5 cm), low-speed movements characteristic of Post 1 and movements that resembled more typical performance (Figures 2C and 2D; Video S3). During Post 3 and Post 4, amplitude and peak speed increased but did not return to pre-lesion levels (Figures 2C and 2D, Pre vs. Post 3–4, amplitude $P < 0.0005$, peak speed $P < 0.0004$). Reach trajectory was also affected. The ratio of reach path length to reach amplitude, or tortuosity, was greatly increased following lesion, with modest improvement over time (Figure 2E, Pre vs. Post 1–4, $P < 0.03$). These behavioral deficits were consistent across individual animals and days (see Figure S1 for individual animal data and statistics). However, not all movement parameters were affected. Forelimb movements observed immediately after the lesion demonstrated increased duration, (Figure 2F, Pre vs. Post 1, $p = 0.002$) but recovered quickly to pre-lesion values (Figure 2F, Pre vs. Post 2–4, $P > 0.30$). A lack of correlation between duration and M1 activity has been observed in other tasks.⁵⁶

Along with kinematics, timing is a critical feature of movement and one that has also been suggested to be a component of M1 and striatal processing.⁵⁷ To assess timing, a separate cohort of animals were trained on a light-cued version of the task (Figure 1B). The inclusion of a cue can also reveal differences due to endogenous vs. exogenous instruction to move. The cued response task differed from the uncued task in that a “go cue” light indicated the end of the “no-movement” inter-trial interval, lasting between 5 and 10 s, chosen from a uniform distribution. Movements initiated before this cue were recorded, but not rewarded. Movements initiated in the final 20% of the inter-trial interval resulted in a 5-s timeout, in which the house lights turned on, and was followed by a new random inter-trial interval. Although there was no maximum response time cutoff, mice shaped their performance to maximize the reward rate while avoiding the punishment periods that followed early movements. As expected, experienced mice initiated movements with a relatively low latency following the cue (669 ± 766.75 ms, median \pm IQR). Kinematics at baseline were similar between versions of the task, although peak speed was lower for animals performing the cued response task (Figures 2D and 2J), presumably due to a speed accuracy trade-off.⁵⁸

The presence of a temporal cueing element did not affect the loss of performance nor the progressive recovery after lesioning M1. Just as in the basic version of the task, we observed a profound deficit in motor performance and kinematics (Figures 2I–2K, Pre vs. Post 1–4 amplitude $P < 0.002$; Post 1–4 peak speed $P < 0.0016$; Post 1–4 tortuosity $P < 0.03$). Reach duration was again only minimally altered Post lesion. Critically, response time deteriorated following M1 lesion (Figure 2H, Pre vs. post 1–3, $P < 0.009$). If a movement was to be responsive to the cue, we would expect its initiation at least within 2 s of go cue onset. Throughout Post 1, no responsive movements were observed. However, as motor performance began to recover after around 10 days post lesion, so too did the response times (Figure 2H, Pre vs. Post 4, uncorrected $p = 0.92$), indicating a role for M1 in motor performance and the timing of movement execution (see Figure S2 for individual

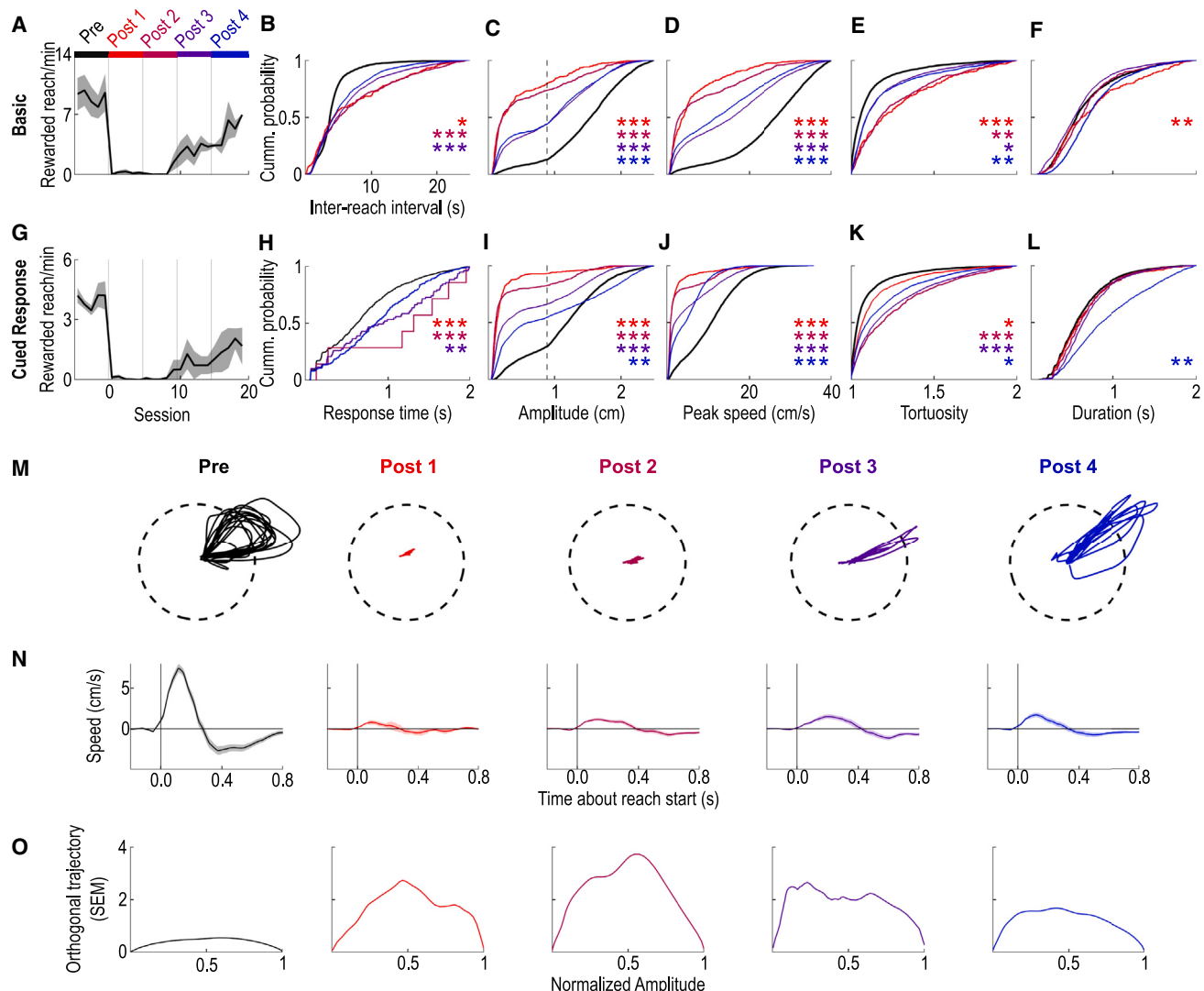


Figure 2. Without M1, task performance is substantially impaired but demonstrates incomplete recovery over time

Top row: basic reaching task. Bottom row: cued reach task.

(A and G) Rewarded reach rate ($\text{mean} \pm \text{SEM}$) over the first 20 min of each session. Sessions are aligned to the day of lesion, day 0. M1 lesion sessions are grouped into 5-day epochs and compared with pre-lesion data using two-sample t tests corrected for multiple comparisons unless otherwise noted. Colors for Pre and Post 1 through Post 4 are conserved across all subsequent figures.

(B) Cumulative histogram of inter-reach intervals.

(C–F and I–L) (C and I) Cumulative histograms of reach amplitude, (D and J) peak speed, (E and K) tortuosity, and (F and L) duration for all detected forelimb movements. Dashed lines in (C) and (I) depict the amplitude threshold for reward (0.9 cm).

(H) Cumulative histogram of response times for the cued response-reaching task. All statistics (B–F, H–L) reflect session averages, not individual reaches. Significant star colors reflect each post-lesion epoch compared with Pre, corrected for multiple comparisons. * $p < 0.05$, ** $p < 0.01$, *** $p < 0.001$.

(M) Randomly selected sample movement trajectories from a pre-lesion session and sessions from each post-lesion epoch. Dashed circle depicts reward threshold (0.9 cm).

(N) Mean \pm SEM of movement trajectory speed from a pre-lesion session and sessions from each post-lesion epoch.

(O) Reach trajectory variability throughout the evolution of the reach. At each point along the reach (0% to 100% of the normalized amplitude), the SEM of deviation orthogonal to reach direction is shown, see STAR Methods for further details.

animal data and statistics). These results support the hypothesis that the motor command to be performed is generated by or conveyed through M1. Post-insult neuroplasticity mechanisms may lead to the improvement of several aspects of performance after some time, potentially as a result of adjacent

cortical areas taking on some of the lost function, as related stroke studies suggest.^{48,53,59,60} Indeed, Kawai and colleagues found no significant effect on task performance at 10 days after lesioning the forelimb motor cortex in rats,²¹ although there were no sessions nor assessment before this time point.

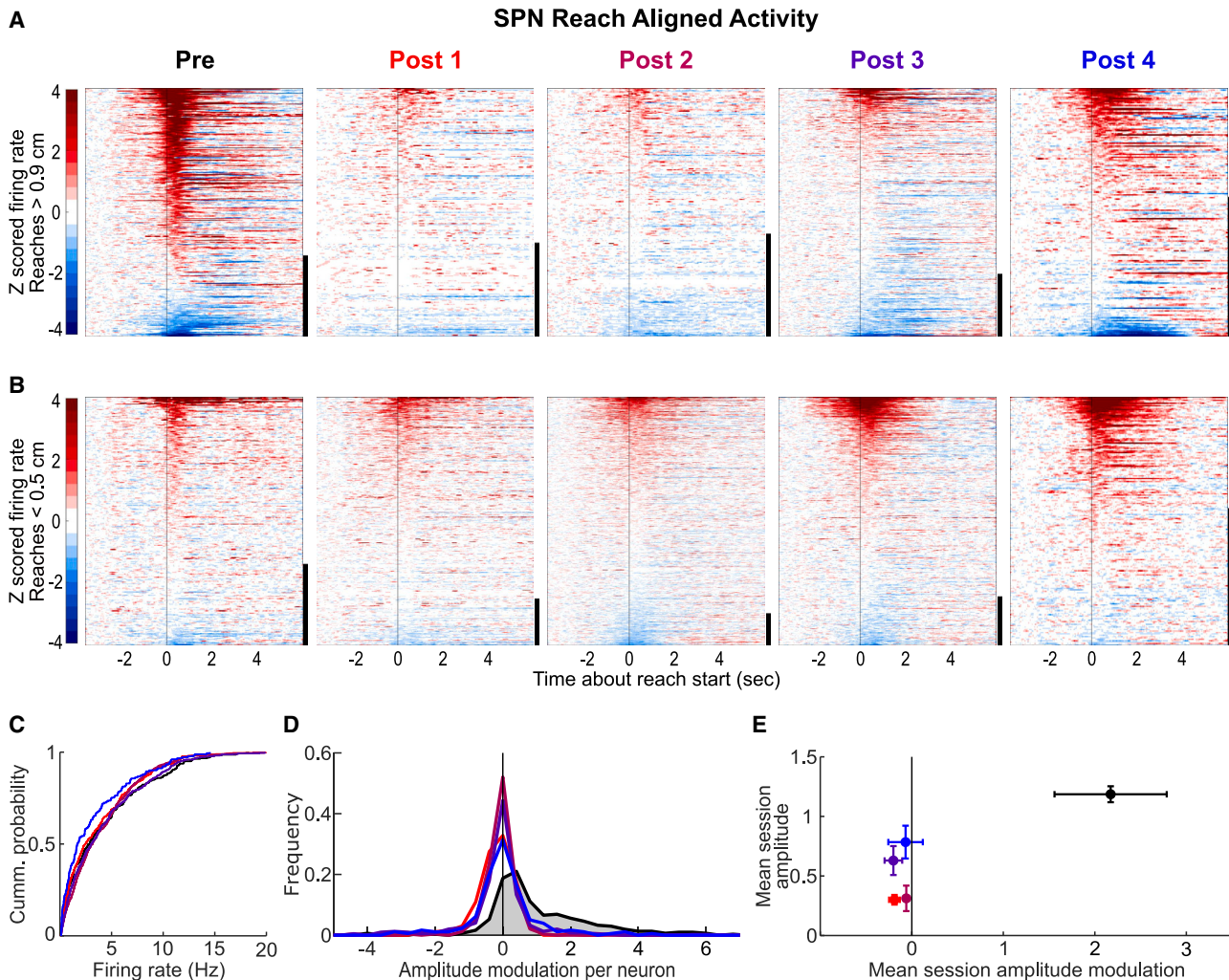


Figure 3. Movement-related SPN activity is absent following bilateral M1 lesions

(A and B) Mean Z scored activity of putative SPNs from all sessions aligned to movement onset for (A) reaches > 0.9 cm and (B) reaches < 0.5 cm. Neurons are sorted by their peak activity between -200 and 600 ms around movement onset. Y scale bar indicates 50 neurons. Neurons that did not respond during a particular reach type are not plotted.

(C) Cumulative histogram depicting baseline firing rates for SPNs across epochs. Each post-lesion epoch is compared with Pre using a two-sample t test corrected for multiple comparisons.

(D) Full distribution of amplitude modulation for all putative SPNs, broken down by post-lesion epoch. The amplitude modulation value for a given neuron is the difference between the absolute mean activity during reaches > 0.9 cm and reaches < 0.5 cm. Only neurons that demonstrated activity during both types of reaches were included.

(E) Comparison of mean amplitude modulation index and amplitude per session (mean \pm SEM).

Motor cortex is selectively responsible for reach-related activity in the striatum

In light of these results, we next asked how movement-related activity in the downstream striatum would be affected by the loss of M1. It has been posited that the storage and generation of learned actions does not require the cortex.²¹ In this case, the removal of M1 should not affect striatal activity, particularly responses related to joystick movement. In contrast, if striatal activity only reflects the modulation of cortical inputs, movement-related activity specifically should be absent following M1 lesion. Thus, we recorded striatal activity before and imme-

diately after lesions of M1 during the same cued response task sessions. Recordings targeted the dorsal striatum in an area that has been shown to receive inputs from M1 and other brain areas.^{35,61}

With M1 intact, 82.0% of putative SPNs demonstrated significant changes in activity around the onset of reaches that exceeded the reward threshold (Figure 3A, Pre; activity quantified in the period $-200:600$ ms relative to reach initiation, see Figure S4 for breakdown of SPN activity by reward outcome and reach amplitude and Figures S7A and S7B for raw firing rate). Modulation of activity in many neurons began prior to movement

onset, consistent with previous observations in uncued reaching studies.^{35,62} Following bilateral lesions of M1, this reach-related striatal activity was greatly reduced. To determine the extent to which reach responsivity was lost, we first determined the fraction of Pre neurons that would be identified as significantly reach modulated if only afforded the reduced suprathreshold reach counts encountered in post-lesion sessions (see STAR Methods for details on iterative subsampling approach). After subsampling pre-lesion sessions to match the mean number of reaches in a given post-lesion epoch, we found that the percent of post-lesion neurons that demonstrated significant reach modulation was greatly reduced and never returned (Figure 3A, Post 2, $p = 0.007$, Post 3 and 4: $Ps < 1 \times 10^{-6}$; chi-squared test, corrected for multiple comparisons and reduced reach count, differences between Post 2–4 fraction of modulated neurons and matched subsampled pre-lesion: 9.55%, 30.55%, and 23.71%, respectively; see STAR Methods for further details). Post 1 had an average suprathreshold reach count of 3 and no significant difference could be resolved (Figure 3A, $p = 0.11$, chi-squared test, corrected for multiple comparisons). These results indicate that these dynamics are M1-dependent and not solely the direct result of thalamic nor other cortical inputs. Throughout these changes, the basal properties of neuronal activity were unaffected. Baseline firing rates of SPNs remained constant (Figure 3C, Pre vs. Post 1–4, uncorrected $Ps > 0.39$, two-sample t test) and Fano factor, a measure of burstiness and firing rate variability, also did not change (Figure S3D, Pre vs. Post 1–4, $Ps > 0.07$, two-sample t test, corrected for multiple comparisons). This consistency in firing properties following lesion was previously observed²⁸ and suggests that a different mechanism governs baseline excitability. These results indicate that neither M1 inputs nor repeated electrode penetrations had an effect on baseline excitability, and this property is governed by thalamic or cortical inputs other than M1.

We also found that the fraction of SPNs demonstrating significant responses for small reaches (<0.5 cm, in line with the bimodal distribution of amplitudes observed post lesion, Figure 2I) increased in successive sessions. In pre-lesion sessions, comparatively few neurons demonstrated responses during small amplitude reaches compared with larger amplitude reaches (Figures 3B and 3D), consistent with several previous studies that observed positive correlations between the magnitude of SPN responses and the vigor of movement.^{35,62,63} Beginning in Post 2, the presence of small-reach responses significantly increased compared with pre-lesion distributions (Figure 3B, Pre vs. Post 2–4 $Ps < 0.001$, Chi-square test, corrected for multiple comparisons). The increase in small-reach responsivity coincides with the increased probability of performing small reaches and greater variance in amplitudes noted previously (Figure 2I).

With reach responsivity increasing over time for both large and small reaches (Figures 3A and 3B), we next determined whether the scaling of striatal activity with reach amplitude was still conserved. Across neurons recorded prior to lesion, we observed this known relationship between firing rate and movement vigor. Specifically, larger amplitude reaches elicited a greater response than smaller reaches by an average margin of 1.28 standard deviations, with a significant positive amplitude modulation (Figure 3D,

$p = 2.4 \times 10^{-12}$, one-sided t test, see Figure S6 for example neurons). However, lesioning eliminated this kinematic relationship across all post-lesion epochs (Figure 3D, Post 1–4 $Ps > 0.89$, one-sided t test). This lack of amplitude modulation stands in contrast to the improvement in mean reach amplitude per session (Figure 3E, Post 1–4, $Ps > 0.64$, one-sided t test, see Figure S6 for individual-session effects). Thus, while some reach responsivity in SPNs returned weeks after the lesion, the new compensatory mechanisms that engaged the striatum did not demonstrate the characteristic kinematic tuning observed in the intact brain.

Although FSIs represent a minority of striatal neurons, they are predominantly concentrated in the dorsal sensorimotor striatum, suggesting that they perform a critical role in motor function.^{64,65} Like SPNs, these neurons are innervated by the M1, thalamus, and other cortical areas. FSIs are thought to play a broad regulatory role over SPN activity,^{66–69} although our understanding of their contribution to *in vivo*, awake behaviors is limited.⁷⁰ Recent studies have revealed that FSI activity encodes the vigor of movement⁶⁵ but also that the influence of FSIs may decline with expertise in a learned task.⁷¹ To ascertain their role within the joystick task, with and without M1 inputs, we examined response profiles of FSIs in the same recording sessions.

Prior to lesion, 71.4% of putative FSIs demonstrated significant reach responses for reaches that surpassed the reward threshold (Figure 4A; see Figure S5 for breakdown of FSI activity by reward outcome and reach amplitude and Figures S7C and S7D for raw firing rate). This reach-related modulation in FSIs was common, typically positive, and began only with the start of the movement, as has been observed in other studies.^{67,72} Following lesion of M1, this reach-related activity in putative FSIs was also greatly reduced and never returned. Again, using subsampled reach trials, we found that significantly fewer post-lesion neurons demonstrated reach responsivity (Figure 4A, Post 2, $p = 0.049$, Post 3 and 4: $Ps < 1 \times 10^{-6}$; chi-squared test, corrected for multiple comparisons. Post 1 was not significantly different; differences between Post 2–4 fraction of modulated neurons and matched subsampled pre-lesion: 14.54%, 35.19%, and 43.20%, respectively). For what reach responsivity that was observed, it was nearly indistinguishable from chance compared with that observed in a temporally scrambled null distribution. (Figure 4A, Post 1 = 21.2%, 99% CI [-6.83, 25.83], Post 2 = 14.6%, 99% CI [-4.46 19.00], Post 3 = 21.0%, 99% CI [-0.78 17.51], Post 4 = 17.1%, 99% CI [1.91 15.82]). This is in contrast to the modest compensatory increase in SPN reach responsivity and may reflect differences in connectivity patterns and computational roles.^{72,73} In contrast to SPNs, FSI activity during small forelimb movements did not change following lesions of M1 (Figure 4B, Pre vs. Post 1–4, uncorrected $Ps > 0.11$, Chi-square test), and together this may indicate that FSI activity may be preferentially linked to goal-oriented movements. However, like SPNs, we found no change in the baseline firing rate nor the Fano factor of putative FSIs following lesion of M1 (Figure 4C, $Ps > 0.20$, two-sample t test, corrected for multiple comparisons, Figure S3D, Pre vs. Post 1–4, uncorrected $Ps > 0.12$, two-sample t test). In the intact brain, FSIs also demonstrated greater activity modulation in association with large amplitude reaches compared with small amplitude reaches (Figure 4D, mean amplitude modulation = 0.58 standard

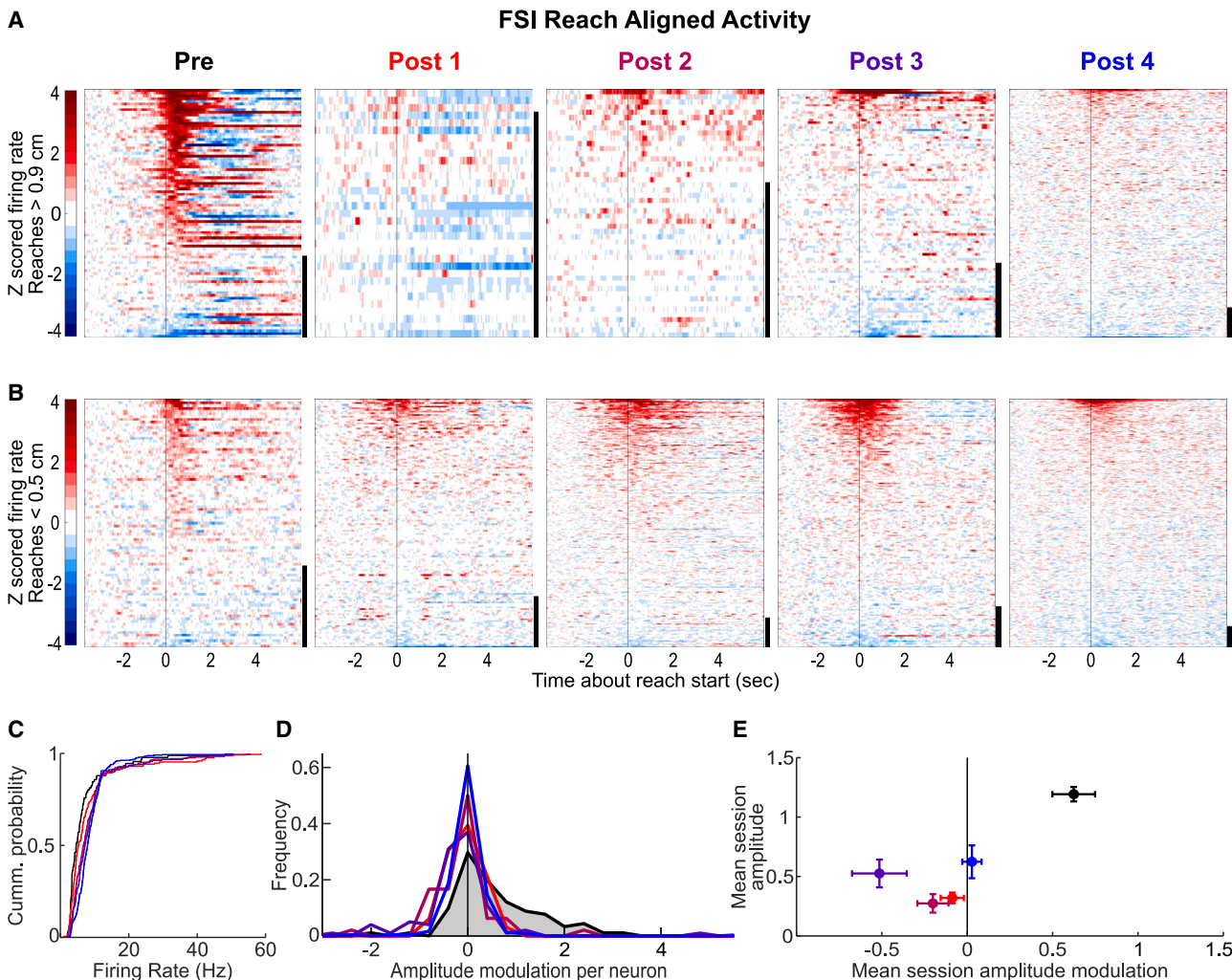


Figure 4. Movement-related FSI activity is absent following bilateral M1 lesions

(A and B) Mean Z scored activity of putative FSIs from all sessions aligned to movement onset for (A) reaches > 0.9 cm and (B) reaches < 0.5 cm. Neurons are sorted by their peak activity between -200 and 600 ms around movement onset. Y scale bar indicates 30 neurons. Neurons that did not respond during the particular reach type are not plotted.

(C) Cumulative histogram depicting baseline firing rates for FSIs across epochs. Each post-lesion epoch is compared with the Pre using a two-sample t test corrected for multiple comparisons.

(D) Full distribution of amplitude modulation for all FSIs, broken down by post-lesion epoch. The amplitude modulation value for a given neuron is the difference between the absolute mean activity during reaches > 0.9 cm and reaches < 0.5 cm. Only neurons that demonstrated activity during both types of reaches were included.

(E) Comparison of mean amplitude modulation index and amplitude per session (mean \pm SEM).

deviations, $p = 5.3 \times 10^{-9}$, one-sided t test). As was observed in SPNs, this pattern of amplitude modulation was lost following M1 lesioning (Figure 4E, Post 1–4 Ps > 0.32 , one-sample t test; see Figure S6 for individual-session effects).

Representation of moment-by-moment reach dynamics in the striatum is permanently lost following M1 lesion

Although the main result of this study is that M1 is critical to learned motor performance and the striatal dynamics that support those movements, these results also indicate that the striatal dynamics observed several days following lesion may reflect a new,

compensatory neuronal state rather than a return to pre-lesion dynamics. We therefore sought to assess what kinematic information was available in striatal population activity before and after bilateral M1 lesions. To this end, we built a feed-forward neural network that attempted to decode the moment-by-moment joystick amplitude from the neural activity across the striatal population. For each decoding iteration, a random subset of 10 neurons per session was selected (see STAR Methods for further details and description of how the number of trials was equalized for each epoch). Using the binned spike counts from each of the neurons in the sample population, we were able to reliably predict

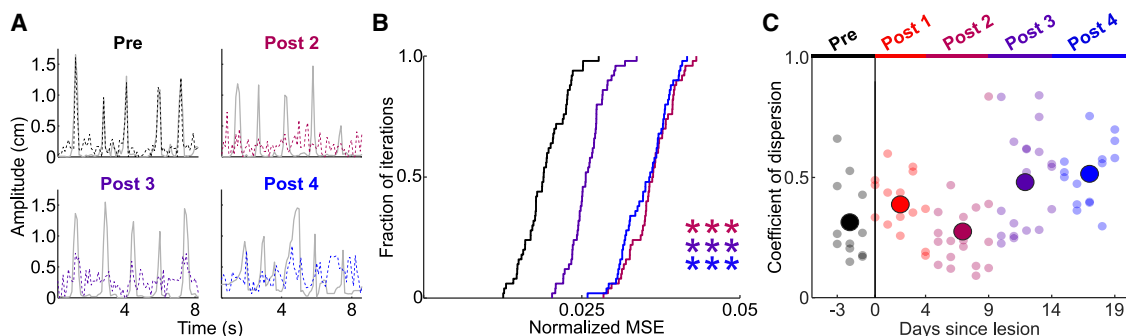


Figure 5. The ability to decode joystick amplitude from striatal population activity is permanently lost following M1 lesions

(A) Example of real (gray) and predicted (dashed color) joystick amplitudes from pre- and post-lesion sessions. Examples are taken from model iterations at the median of the performance distributions for each post-lesion epoch, having the following normalized MSE values: Pre: 0.018, Post 2: 0.036, Post 3: 0.025, and Post 4: 0.035. Post 1 was excluded due to insufficient number of reaches meeting criteria (see STAR Methods).

(B) Distribution of model performance across multiple iterations. Reaches and neurons were subsampled to allow comparison with Post 2. Each epoch was run 10 times through the model with 10 randomly subsampled neurons for each iteration. This was repeated 50 times with randomly subsampled reaches to develop the full distribution plotted. *** $p < 0.001$.

(C) Amplitude coefficient of dispersion per session relative to day of lesion (small dots). Larger dots depict post-lesion epoch means.

joystick position in pre-lesion sessions (median normalized MSE of 0.018, Figure 5B). Following bilateral lesions of M1, the ability to decode joystick position was lost and was never regained, despite the considerable improvements in task performance observed by days 10–19. This pattern of effects was also observed if 30 neurons were used (Figure S8).

To better understand why we were unable to resolve the execution of a reach, we reassessed performance kinematics in the later post-lesion sessions. We examined the trial-by-trial behavioral distributions and discovered that the late-stage increase in rewarded task performance (Figures 2A and 2G) was accompanied by an increase in amplitude variability (Figure 5C, Pre vs. Post 3 or 4, $p = 0.052$ and 0.003, respectively, two-sample t test, corrected for multiple comparisons). Thus, the improved ability to perform rewarded reaches at this stage in recovery does not reflect a return to baseline performance. Mice were able to generate movements but without the kinematic control to accurately target movements to just above amplitude reward threshold, as in pre-lesion performance. Although this pattern of behavior may be the result of an alternative cognitive strategy to earn rewards, we cannot rule out that the inability to control movement vigor may be due to the failure of compensatory circuits to engage the striatum and its motor control functions.^{29,36,74} Thus, without the striatum acting to modulate the kinematic gain of the descending motor commands arising from compensatory circuits, likely from the peri-lesional cortex,^{48,53,59,75} lesioned mice may be unable to appropriately and effectively modulate the kinematics of their reaches. Together with our single-unit activity and the changes in amplitude modulation index, these results demonstrate that, in the absence of M1, striatal activity alone is not sufficient to produce intact goal-directed reaching.

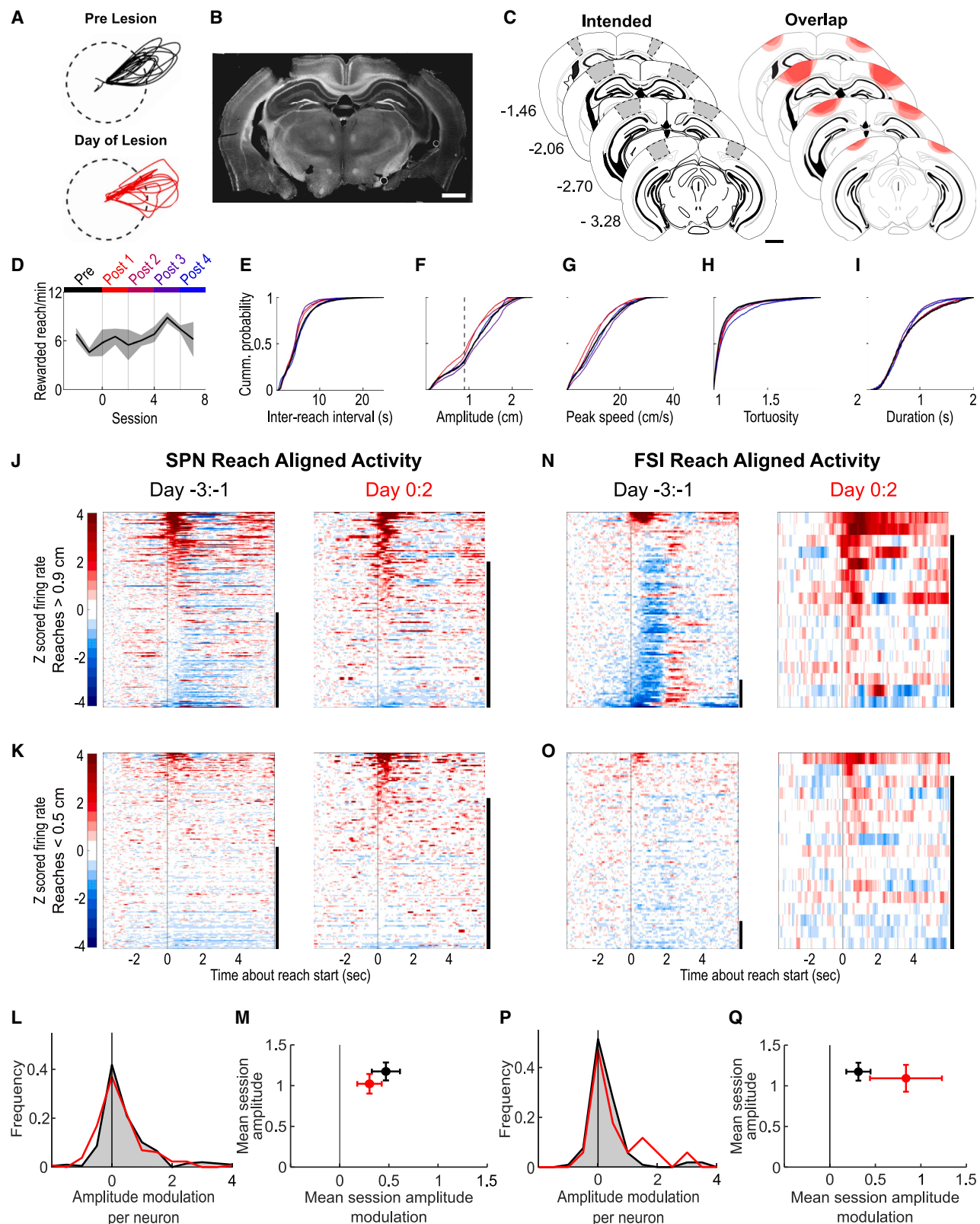
PPC lesions do not affect reach performance nor striatal representation

To more directly control for the possibility that cortical lesions may produce wide-ranging effects, including inflammation and

functional deafferentation or diaschisis,^{76–78} we induced comparably sized bilateral lesions centered in PPC. This intervention also provides the opportunity to gain a greater understanding of the broader motor control circuit. PPC is a sensorimotor area that has also been shown to contribute to reaching movements,^{79–81} but it is unclear how PPC activity supports the generation of these movements. To avoid perceptual confounds owing to visual processing in PPC, the basic uncued version of the task was used (Video S4).

In sharp contrast to behavior after M1 lesions, mice demonstrated no performance deficits following PPC lesions (Video S5). On the day of lesion, we observed no changes in trial performance (Figures 6D and 6E, Pre vs. Post 1–4, trial rate and inter-reach interval $P_s > 0.5$, two-sample t test, corrected for multiple comparisons) nor reach kinematics (Figures 6F–6I, reach amplitude, peak speed, duration, and tortuosity, Pre vs. Post 1–4, $P_s > 0.25$, two-sample t test, corrected for multiple comparisons). Given the lack of effect of PPC lesions, particularly relative to M1 lesions, mice receiving PPC lesions were only run for 7 days post lesion and only on the basic center-out task (see Figure S9 for individual animal data and statistics). After the day of lesion, no subsequent changes in performance (Figures 6D and 6E, $P_s > 0.18$, two-sample t test, corrected for multiple comparisons) nor reach kinematics (Figures 6F–6I, Pre vs. Post 1–4, $P_s > 0.35$, two-sample t test, corrected for multiple comparisons) were observed. These results are comparable with other rodent reaching tasks that found no behavioral deficits following PPC insult.⁷⁷

Despite a lack of discernible behavioral effects, striatal encoding of movement may have been altered due to the loss of PPC input or general insult to the brain. However, we found no changes in reach-related responsivity in SPNs nor in FSIIs following bilateral lesions of PPC (Figure 6, day –3: –1 vs. day 0:2, $P_s > 0.48$ for all comparisons, chi-square test). We note that these mice performed the basic uncued task. We also found that there was no change in the extent of amplitude modulation found in SPNs (Figure 6M, day –3: –1 vs. day 0:2, $p = 0.39$,



(legend on next page)

two-sample t test) nor FSIs (*Figure 6Q*, day –3: –1 vs. day 0:2, $p = 0.15$, two-sample t test) following lesions of PPC. These negative results indicate that the effects of the M1 lesion are unlikely to be due to non-specific complications arising from the procedure, even on the day of lesion. Additionally, while the PPC likely plays a role in movement planning, particularly when evidence accumulation is involved,^{79,82,83} it is not critical for the generation of motor commands themselves nor their representation in striatum. This control for generalized lesion effects also provides an informative step toward understanding the broader cortical control of movement and reinforces the role of M1 in the generation of a motor command and its concomitant activity in striatum.

M1 lesions impair untrained motor decisions in a manner similar to FOG

In both versions of the reaching task, lesions to M1 prevented the execution of the learned, skilled motor action. From these experiments, however, we cannot determine whether these findings also generalize to untrained movements and decisions. To further understand the role of M1 in the selection and execution of actions, we examined spontaneous movement of the same M1-lesioned mice. Within 30 min of recovery from lesion surgery, mice could locomote and groom without obvious impairment (*Videos S6* and *S9*). However, we also observed profound freezing behavior when external contexts necessitated updating of their motor state (*Videos S7* and *S8*). To quantify this initial observation, M1-lesioned mice were allowed to navigate through a T-maze without any reward. Mice placed at base of the T-maze will naturally begin to locomote, decelerating briefly upon approaching the junction while deciding in which direction to turn (*Video S6*). We measured the amount of time mice spent along the T-maze hallways in M1-lesioned or unoperated control animals (*Figures 7B–7E*). We partitioned the T-maze into 5-cm-long divisions, numbered successively from 1 at the base to 10 at the intersection, with 11 through 13 extending in both directions away from the intersection (*Figure 7B* inset, image stills in *Figure 7A* depict T partitions 9, 10, and the left and right 11).

Following M1 lesion, mice demonstrated extended locomotor freezing as they arrived at the threshold of the crossing hallway, amounting to tens of seconds fixed in place (lesion vs. unoper-

ated control mice difference in occupancy time: position 9 = 68.89 s, $p = 0.0014$; position 10 = 24.18 s, $p = 0.009$, two-sample t test). During this time, mice were frozen in mid-step rather than stopped to rest or groom. *Figure 7A* provides an example. Even though the video frames shown are 10 s apart, they almost appear to be copies of the same mid-stride frame (see *Video S7*). After some time, mice eventually proceeded down a selected hallway. This effect occurred despite locomotor speed being normal—e.g., there was no difference in occupancy time as mice traversed through the other portions along the initial hallway (difference in mean occupancy time across positions 1–8: 5.09 s; $P > 0.11$ for any individual division, two-sample t test). Through subsequent sessions, we observed that freezing lessened. By days 10–15 (*Figure 7E*, Post 3), lesion and control animals that had experienced the same number of T-maze sessions demonstrated comparable movement through the T-maze. We observed qualitatively similar deficits when navigating minor obstructions—e.g., a small block placed in the middle of the hallway (*Video S8*), which typically does not impede a mouse. Intact locomotion has also been reported during bilateral optogenetic inhibition of M1 in the mouse, where it was shown that M1 is only required for the updating of motor commands in response to a change in context when navigating a virtual corridor.¹⁹ In both cases, the subject is capable of locomotion—demonstrating that the deficit is not one of physical limitation. A similar motoric set switching disorder, called freezing of gait (FOG), is associated with several clinical conditions.⁸⁴

DISCUSSION

To establish the functional contribution of motor cortex to the dynamics of striatal populations and behaviors, we monitored neural and behavioral activity on a daily basis, both before and after lesioning the CFA of M1. In the days following the lesion, we discovered that both SPN and FSI striatal neurons lost their movement-related activity, even as the ability to successfully perform the task slowly returned. In the neural activity that did return, we found that it did not encode movement vigor and could not be used to predict movement trajectories. The inability to execute motor decisions was observed in both self-paced and cued trained actions, as well as in untrained behaviors when

Figure 6. Bilateral parietal lesions do not affect the ability to reach, reaching kinematics, nor motor representations in the striatum

- (A) Randomly selected sample movement trajectories from a pre-lesion session (top) and the day of PPC (bottom). Dashed circle depicts reward threshold (0.9 cm).
- (B) Example bilateral PPC lesion (–2.10 mm relative to bregma). Scale bar depicts 1 mm.
- (C) Reconstruction of bilateral aspiration lesions centered on PPC. Left: coronal sections from a standard mouse brain depicting the extent of PPC. Numeric values depict distance from bregma in mm. Right: the extent and overlap of the aspiration lesions from the four lesioned mice. Scale bar depicts 1 mm.
- (D) Rewarded reach rate (mean ± SEM) over the first 20 min of each session. Sessions are aligned to the day of lesion, day 0. Post-lesion sessions are grouped into 2-day epochs and compared with pre-lesion data. Colors for Pre and Post epochs are conserved across all *Figure 6* panels.
- (E–I) Cumulative histograms depicting distribution of reach performance metrics. Dashed line in (F) depicts the amplitude threshold for reward (0.9 cm).
- (J and K) Average Z scored activity of putative SPNs from all sessions aligned to movement onset for reaches (J) > 0.9 cm or (K) < 0.5 cm in the 3 days prior and 3 days following PPC lesions, starting on the day of the lesion. Same conventions as *Figure 3*. Y scale bar depicts 50 neurons.
- (L) Full distribution of all putative SPN amplitude modulation indexes. Only neurons that were recorded during reaches > 0.9 cm (J) and < 0.5 cm (K) were included.
- (M) Comparison of mean SPN amplitude modulation index and amplitude per session (mean ± SEM).
- (N and O) Average Z scored activity of putative FSIs from all sessions aligned to movement onset for reaches > 0.9 cm (N) and reaches < 0.5 cm (O) in the 3 days prior and 3 days following PPC lesions, starting on the day of the lesion. Same conventions as *Figure 3*. Y scale bar depicts 15 neurons.
- (P) Full distribution of all putative FSI amplitude modulation indexes. Only neurons that were recorded during reaches > 0.9 cm (N) and < 0.5 cm (O) were included.
- (Q) Comparison of mean FSI amplitude modulation index and amplitude per session (mean ± SEM).

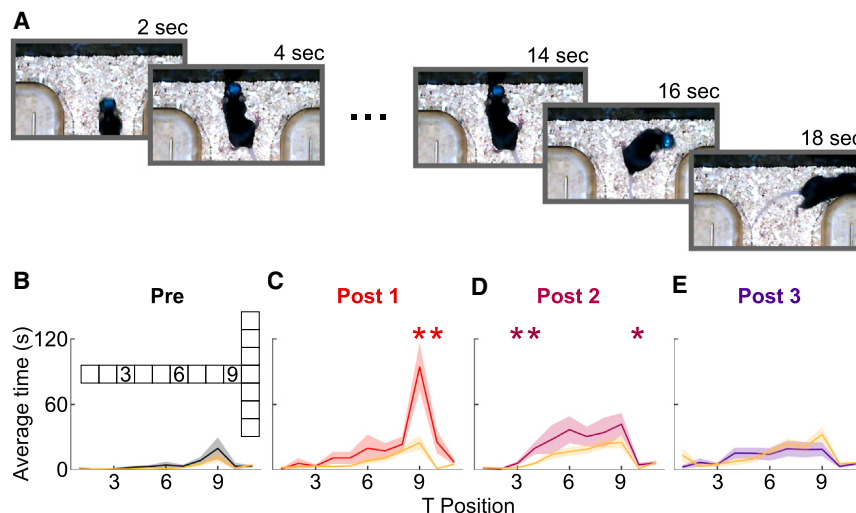


Figure 7. The loss of M1 results in locomotor freezing at the junction of T-maze hallways

(A) Video stills demonstrating freezing of gait at the threshold of the T-maze hallway prior to continuing to the chosen arm ([Video S7](#)).

(B–E) Time spent (mean \pm SEM) along segments of the central axis of the T-maze compared with unoperated controls (gold) for Pre (B), Post 1 (C), Post 2 (D), and Post 3 (E) (two-sample t test, * P s < 0.05, for that segment). Inset in (B) depicts T positions, each box depicts 5 cm.

an updating of the selected context was required at the end of the hallway in a T-maze. Finally, control lesions of parietal cortex were unable to produce these behavioral and neural deficits, indicating that our results are not the consequence of diaschisis or other generalized lesion effects. These discoveries point to a circuit computation in which M1 is necessary for determining and generating the action command, with the striatum receiving this motor command for further modulation—as suggested by several models of corticostriatal function, including the history-dependent gain model.^{29,31}

Overall, our work aligns well with related studies of M1 lesions across species and approaches.^{85–88} Despite the caveat that our lesioning method affects fibers of passage, alternative methods have yielded similar results. For instance, Guo and colleagues utilized transient photoactivation and also found that M1 was necessary to generate the next motor command in a reach-to-grasp task.¹⁸ Our work also bears a similarity to lesions of the motor cortex in human and non-human primates (see Darling et al.¹⁵ for a thorough review). There has been some question of the functional homology of M1 between rodents and primates due to their cytoarchitectural and behavioral repertoire differences.²³ Though differences are clearly present, our results point to a shared functional foundation: the flexible control of motor behavior requires the contributions of M1.

Recently, a series of contrary studies reported that lesions of rodent M1 have no effect on learned behavior or dorsal striatal activity.^{21,28} A few informative observations can be made regarding differences in approach when comparing our findings. First, these studies did not analyze behavior until 10 days after lesion. The result of an intervention is typically most accurate shortly following the completion of the manipulation. With the progression of time, the observed effects may change as behavioral and physiological compensation take place. These later effects are more likely to reflect large-scale plasticity events rather than the brain's inherent dynamics. The state of the brain following this compensation may be a poor match of the initial, pre-manipulation state.⁸⁹ Across species, both stroke and lesion models have shown that considerable adaptation takes place in the first few days post insult^{90–92}—even in the absence of

rehabilitation.⁹³ From an evolutionary perspective, the nervous system is well-motivated to recover motor function by whatever means are necessary, as it is critical to an animal's survival. Gharabawie and Whishaw specifically observed that in M1-lesioned rats, performance in a reaching task achieved pre-lesion levels at or around day 10.⁷⁷ Indeed, the immediate effects observed in Post 1 align with optogenetic inactivation results, while at the +10 day post-lesion time points we observed that behavioral and neural dynamics appear to be largely recovered. In our results, it is only through deeper analysis of the trial-by-trial kinematic and neural features that we observe that the recovered brain and behavioral dynamics do not match pre-lesion values.

We also recognize an emerging appreciation of the degree to which motor processes may change with excessive training.⁹⁴ Although not explicitly stated, plots depicting over 25,000 training trials over as many as 60 sessions occurred in these studies. An organism may become a skilled “expert” in a task after considerable training, but further practice may shift the execution of the action to a more crystalized state wherein the flexibility of performance, often ascribed to motor cortex, is supplanted by automaticity.⁹⁵ Hwang and colleagues found that optogenetic inactivation of M1 only produced behavioral deficits in a skilled motor task for animals that may be relatively expert, but not overtrained, in the task.²² They also observed that the consistency of movement-related activity in M1 decreased with expertise. For comparison, this “late learning” state described animals with over 60 training sessions, while our mice were trained 46.7 sessions on average, with potentially far fewer total trials across these sessions. Together with the extensively trained animals in the aforementioned studies,^{21,28} these results provide strong support for the notion that M1 can progressively disengage after prolonged practice of a skilled motor action. Indeed, the pattern of results observed in the T-maze may reflect this distinction for automatized behaviors. The ability to walk is preserved and was only interfered with when the flexibility to change motor state was required. Thus, M1 would instruct the dedicated downstream brainstem and spinal circuits to execute the action it selects.⁹⁶

Finally, there are important differences between these behaviors. Although the forelimb is an important locus of movement in the behaviors from all of the studies mentioned above, the raising and lowering of the torso plays a major, if not predominant, role in lever pressing. As such, lesions to the forelimb area of M1 may

spare some of the full-body representations required for lever press execution. Indeed, we found here that locomotion, which utilizes muscles of the four limbs and torso, was still largely intact following M1 lesion. Lever pressing is also not a dexterous task. Although our mice do grasp the joystick, their movements are not dexterous in the traditional or clinical sense of requiring fine manipulation of the digits or a particular coordinated pattern of movement.⁹⁷ Moreover, despite lesions to M1, mice appeared to grasp the joystick without difficulty or clumsiness (*Video S2*). If necessary, any grip would suffice to displace the joystick, including an open-handed push or close-fisted punch. Most importantly, M1 lesion deficits are not limited to the trained task. Although the execution of walking itself was unaffected, animals failed to switch motor state in the performance of this non-dexterous, untrained, and unrewarded behavior of walking.

M1 is always required for skilled movements. More broadly, these results suggest that the encoding of the selected action plan occurs upstream of the striatum. If the neural representations and function of the striatum do not depend on input from motor cortex, there should be no differences observed when actions are performed following M1 lesions. Additionally, if the activation of striatal neurons selects the action to be performed, it is difficult to hypothesize why no striatal activity accompanied reaches that were performed in the week following the lesion. Although prolonged activation of the striatum is sufficient to induce contralateral or ipsilateral turning,²⁶ M1-lesioned mice exhibit profound difficulties in selecting to perform a turn, despite having an intact striatum.

Our T-maze results following M1 lesion are consistent with a clinical condition called FOG, affecting millions of people. FOG is a motoric set switching disorder in which patients often report that their decision to walk is blocked.⁸⁴ The failure of motoric set switching that characterizes FOG is encountered particularly when attempting to turn, cross the threshold of a doorway, and maneuver in other scenarios where a change of motor plan is required.⁹⁸ Although FOG is commonly observed in Parkinson's disease following the loss of dopaminergic inputs throughout the brain, it is a hallmark of several neurophysiological disorders, and recent clinical studies suggest that FOG may result from M1 dysfunction that accompanies Parkinson's disease.^{99,100} Critically, excitatory stimulation of M1 has been shown to be a beneficial intervention.¹⁰¹ The T-maze hall junction provides the environmental context that requires mice to make a motoric decision, which left the animal unable to move, sometimes for minutes. These results point to M1's important role in executing motor plans and its potential role in FOG.

Finally, the neurobehavioral trajectory of recovery may provide the most important insights. Peri-lesional cortex is known to be instrumental in the recovery of function, taking on the neural representations of the lost cortex in the days following insult,^{48,53,59,75,90} while lesion-related changes in striatum significantly lag.¹⁰² In our study, the ability to generate reaches and turns was regained after only a short delay, around day 10 post lesion. This timing is consistent with the compensatory role of the peri-lesional cortex taking over the role of M1 in executing these actions. If peri-lesional areas of the cortex have taken on the role of executing motor commands, it is reasonable to expect that downstream striatal neurons would

exhibit the modest recovery of reach responsivity we observed in Post 3 and Post 4. Additionally, the difference in activity recovery between SPNs and FSIs may be instructive. Compared with SPNs, FSIs demonstrated little to no improvement in reach responsivity despite robust pre-lesion responses in both populations. FSIs are less promiscuous in their range of corticostriatal inputs than SPNs.⁷³ Some of the great diversity of SPN inputs from across cortical areas would now be driving reach commands. However, even in later sessions, we observed that kinematic control of reaches and kinematic encoding in striatal neurons were absent. Without considerable synaptic re-tuning, it is unlikely that the striatum would be capable of properly assigning kinematic modulation to the new pattern of innervation it receives. Indeed, considerable cortical axon sprouting and synaptic plasticity is observed in the subsequent weeks,¹⁰² and this may support the continued restoration of behavioral performance. These results suggest a reappraisal of recent studies and are indicative of the cortex being responsible for the generation of the motor command to be performed, while the striatum modulates the performance of that action.

STAR METHODS

Detailed methods are provided in the online version of this paper and include the following:

- [KEY RESOURCES TABLE](#)
- [RESOURCE AVAILABILITY](#)
 - Lead contact
 - Materials availability
 - Data and code availability
- [EXPERIMENTAL MODEL AND STUDY PARTICIPANT DETAILS](#)
- [METHOD DETAILS](#)
 - Joystick tasks
 - Experimental setup
 - Surgical procedures
 - Unrewarded T-maze task
 - Electrophysiology data acquisition
 - Histology
- [QUANTIFICATION AND STATISTICAL ANALYSIS](#)
 - Joystick kinematics analysis
 - Striatal cell identification
 - Electrophysiology data analysis
 - Joystick decoding from striatal activity
 - T-Maze analysis
 - Statistical testing

SUPPLEMENTAL INFORMATION

Supplemental information can be found online at <https://doi.org/10.1016/j.neuron.2024.07.022>.

ACKNOWLEDGMENTS

We would like to thank Parley Belsey for technical assistance and Drs. Aryn Gittis, Alexander Friedman, and Rob Turner and members of the Yttri lab for comments on the manuscript. This work was supported by the Brain Research Foundation Fay/Frank Seed Grant, the Charles E. Kaufman Foundation New Investigator Award, and the Whitehall Foundation.

AUTHOR CONTRIBUTIONS

M.A.N. conceived the study; acquired, analyzed, and interpreted the data; created the analysis software; and drafted the manuscript. E.A.Y. conceived the study, analyzed and interpreted the data, and drafted the manuscript.

DECLARATION OF INTERESTS

The authors declare no competing interests.

Received: November 1, 2023

Revised: March 28, 2024

Accepted: July 26, 2024

Published: August 20, 2024

REFERENCES

- Huber, D., Gutnisky, D.A., Peron, S., O'Connor, D.H., Wiegert, J.S., Tian, L., Oertner, T.G., Looger, L.L., and Svoboda, K. (2012). Multiple dynamic representations in the motor cortex during sensorimotor learning. *Nature* 484, 473–478. <https://doi.org/10.1038/nature11039>.
- Peters, A.J., Chen, S.X., and Komiyama, T. (2014). Emergence of reproducible spatiotemporal activity during motor learning. *Nature* 510, 263–267. <https://doi.org/10.1038/nature13235>.
- Russo, A.A., Bittner, S.R., Perkins, S.M., Seely, J.S., London, B.M., Lara, A.H., Miri, A., Marshall, N.J., Kohn, A., Jessell, T.M., et al. (2018). Motor cortex embeds muscle-like commands in an untangled population response. *Neuron* 97, 953–966.e8. <https://doi.org/10.1016/J.NEURON.2018.01.004>.
- Pearce, T.M., and Moran, D.W. (2012). Strategy-dependent encoding of planned arm movements in the dorsal premotor cortex. *Science* 337, 984–988. <https://doi.org/10.1126/science.1220642>.
- Graziano, M.S.A., Taylor, C.S.R., and Moore, T. (2002). Complex Movements Evoked by Microstimulation of Precentral Cortex. *Neuron* 34, 841–851. [https://doi.org/10.1016/S0896-6273\(02\)00698-0](https://doi.org/10.1016/S0896-6273(02)00698-0).
- Hoffman, D.S., and Strick, P.L. (1995). Effects of a primary motor cortex lesion on step-tracking movements of the wrist. *J. Neurophysiol.* 73, 891–895. <https://doi.org/10.1152/JN.1995.73.2.891>.
- Scott, S.H., Gribble, P.L., Graham, K.M., and Cabel, D.W. (2001). Dissociation between hand motion and population vectors from neural activity in motor cortex. *Nature* 413, 161–165. <https://doi.org/10.1038/35093102>.
- Schwartz, A.B. (1994). Distributed motor processing in cerebral cortex. *Curr. Opin. Neurobiol.* 4, 840–846. [https://doi.org/10.1016/0959-4388\(94\)90132-5](https://doi.org/10.1016/0959-4388(94)90132-5).
- Gallego, J.A., Perich, M.G., Miller, L.E., and Solla, S.A. (2017). Neural Manifolds for the Control of Movement. *Neuron* 94, 978–984. <https://doi.org/10.1016/J.NEURON.2017.05.025>.
- Cheney, P.D., and Fetz, E.E. (1985). Comparable patterns of muscle facilitation evoked by individual corticomotoneuronal (CM) cells and by single intracortical microstimuli in primates: evidence for functional groups of CM cells. *J. Neurophysiol.* 53, 786–804. <https://doi.org/10.1152/JN.1985.53.3.786>.
- Kalaska, J.F. (2009). From Intention to Action: Motor Cortex and the Control of Reaching Movements. *Adv. Exp. Med. Biol.* 629, 139–178. https://doi.org/10.1007/978-0-387-77064-2_8.
- Brown, A.R., and Teskey, G.C. (2014). Motor Cortex Is Functionally Organized as a Set of Spatially Distinct Representations for Complex Movements. *J. Neurosci.* 34, 13574–13585. <https://doi.org/10.1523/JNEUROSCI.2500-14.2014>.
- Lashley, K.S. (1920). Studies of cerebral function in learning. *Psychobiology* 2, 55–135. <https://doi.org/10.1037/H0071866>.
- Lawrence, D.G., and Kuypers, H.G.J.M. (1968). THE FUNCTIONAL ORGANIZATION OF THE MOTOR SYSTEM IN THE MONKEYII. THE EFFECTS OF LESIONS OF THE DESCENDING BRAIN-STEM PATHWAYS. *Brain* 91, 15–36. <https://doi.org/10.1093/BRAIN/91.1.15>.
- Darling, W.G., Pizzimenti, M.A., and Morecraft, R.J. (2011). FUNCTIONAL RECOVERY FOLLOWING MOTOR CORTEX LESIONS IN NON-HUMAN PRIMATES: EXPERIMENTAL IMPLICATIONS FOR HUMAN STROKE PATIENTS. *J. Integr. Neurosci.* 10, 353–384. <https://doi.org/10.1142/S0219635211002737>.
- Ramanathan, D.S., Guo, L., Gulati, T., Davidson, G., Hishinuma, A.K., Won, S.J., Knight, R.T., Chang, E.F., Swanson, R.A., and Ganguly, K. (2018). Low-frequency cortical activity is a neuromodulatory target that tracks recovery after stroke. *Nat. Med.* 24, 1257–1267. <https://doi.org/10.1038/s41591-018-0058-y>.
- Galiñanes, G.L., Bonardi, C., and Huber, D. (2018). Directional Reaching for Water as a Cortex-Dependent Behavioral Framework for Mice. *Cell Rep.* 22, 2767–2783. <https://doi.org/10.1016/J.CELREP.2018.02.042>.
- Guo, J.Z., Graves, A.R., Guo, W.W., Zheng, J., Lee, A., Rodríguez-González, J., Li, N., Macklin, J.J., Phillips, J.W., Mensh, B.D., et al. (2015). Cortex commands the performance of skilled movement. *eLife* 4, e10774. <https://doi.org/10.7554/eLife.10774>.
- Heindorf, M., Arber, S., and Keller, G.B. (2018). Mouse Motor Cortex Coordinates the Behavioral Response to Unpredicted Sensory Feedback. *Neuron* 99, 1040–1054.e5. <https://doi.org/10.1016/J.NEURON.2018.07.046>.
- Morandell, K., and Huber, D. (2017). The role of forelimb motor cortex areas in goal directed action in mice. *Sci. Rep.* 7, 15759. <https://doi.org/10.1038/s41598-017-15835-2>.
- Kawai, R., Markman, T., Poddar, R., Ko, R., Fantana, A.L., Dhawale, A.K., Kampff, A.R., and Ölveczky, B.P. (2015). Motor Cortex Is Required for Learning but Not for Executing a Motor Skill. *Neuron* 86, 800–812. <https://doi.org/10.1016/j.neuron.2015.03.024>.
- Hwang, E.J., Dahlen, J.E., Hu, Y.Y., Aguilar, K., Yu, B., Mukundan, M., Mitani, A., and Komiyama, T. (2019). Disengagement of motor cortex from movement control during long-term learning. *Sci. Adv.* 5, eaay0001. <https://doi.org/10.1126/sciadv.aay0001>.
- Warriner, C.L., Fageiry, S.K., Carmona, L.M., and Miri, A. (2020). Towards Cell and Subtype Resolved Functional Organization: Mouse as a Model for the Cortical Control of Movement. *Neuroscience* 450, 151–160. <https://doi.org/10.1016/J.NEUROSCIENCE.2020.07.054>.
- Mink, J.W. (1996). The basal ganglia: focused selection and inhibition of competing motor programs. *Prog. Neurobiol.* 50, 381–425. [https://doi.org/10.1016/s0301-0082\(96\)00042-1](https://doi.org/10.1016/s0301-0082(96)00042-1).
- Hikosaka, O., Takikawa, Y., and Kawagoe, R. (2000). Role of the basal ganglia in the control of purposive saccadic eye movements. *Physiol. Rev.* 80, 953–978. <https://doi.org/10.1152/physrev.2000.80.3.953>.
- Kravitz, A.V., Freeze, B.S., Parker, P.R.L., Kay, K., Thwin, M.T., Deisseroth, K., and Kreitzer, A.C. (2010). Regulation of parkinsonian motor behaviours by optogenetic control of basal ganglia circuitry. *Nature* 466, 622–626. <https://doi.org/10.1038/nature09159>.
- Tai, L.H., Lee, A.M., Benavidez, N., Bonci, A., and Wilbrecht, L. (2012). Transient stimulation of distinct subpopulations of striatal neurons mimics changes in action value. *Nat. Neurosci.* 15, 1281–1289. <https://doi.org/10.1038/nn.3188>.
- Dhawale, A.K., Wolff, S.B.E., Ko, R., and Ölveczky, B.P. (2021). The basal ganglia control the detailed kinematics of learned motor skills. *Nat. Neurosci.* 24, 1256–1269. <https://doi.org/10.1038/s41593-021-00889-3>.
- Dudman, J.T., and Krakauer, J.W. (2016). The basal ganglia: From motor commands to the control of vigor. *Curr. Opin. Neurobiol.* 37, 158–166. <https://doi.org/10.1016/j.conb.2016.02.005>.
- Nelson, A.B., and Kreitzer, A.C. (2014). Reassessing models of basal ganglia function and dysfunction. *Annu. Rev. Neurosci.* 37, 117–135. <https://doi.org/10.1146/ANNUREV-NEURO-071013-013916>.

31. Yttri, E.A., and Dudman, J.T. (2018). A Proposed Circuit Computation in Basal Ganglia: History-Dependent Gain. *Mov. Disord.* 33, 704–716. <https://doi.org/10.1002/mds.27321>.
32. Albin, R.L., Young, A.B., and Penney, J.B. (1989). The functional anatomy of basal ganglia disorders. *Trends Neurosci.* 12, 366–375. [https://doi.org/10.1016/0166-2236\(89\)90074-X](https://doi.org/10.1016/0166-2236(89)90074-X).
33. McGregor, M.M., and Nelson, A.B. (2019). Circuit Mechanisms of Parkinson's Disease. *Neuron* 101, 1042–1056. <https://doi.org/10.1016/J.NEURON.2019.03.004>.
34. Gittis, A.H., and Yttri, E.A. (2018). Translating Insights From Optogenetics To Therapies For Parkinson's Disease. *Curr. Opin. Biomed. Eng.* 8, 14–19. <https://doi.org/10.1016/J.COBME.2018.08.008>.
35. Yttri, E.A., and Dudman, J.T. (2016). Opponent and bidirectional control of movement velocity in the basal ganglia. *Nature* 533, 402–406. <https://doi.org/10.1038/nature17639>.
36. Turner, R.S., and Desmurget, M. (2010). Basal ganglia contributions to motor control: A vigorous tutor. *Curr. Opin. Neurobiol.* 20, 704–716. <https://doi.org/10.1016/j.conb.2010.08.022>.
37. Marsden, C.D., and Obeso, J.A. (1994). The functions of the basal ganglia and the paradox of stereotaxic surgery in Parkinson's disease. *Brain* 117, 877–897. <https://doi.org/10.1093/BRAIN/117.4.877>.
38. Gerfen, C.R. (1992). The neostriatal mosaic: multiple levels of compartmental organization in the basal ganglia. *Annu. Rev. Neurosci.* 15, 285–320. <https://doi.org/10.1146/annurev.ne.15.030192.001441>.
39. Kiritani, T., Wickersham, I.R., Seung, H.S., and Shepherd, G.M.G. (2012). Hierarchical Connectivity and Connection-Specific Dynamics in the Corticospinal-Corticostriatal Microcircuit in Mouse Motor Cortex. *J. Neurosci.* 32, 4992–5001. <https://doi.org/10.1523/JNEUROSCI.4759-11.2012>.
40. Shepherd, G.M.G. (2013). Corticostriatal connectivity and its role in disease. *Nat. Rev. Neurosci.* 14, 278–291. <https://doi.org/10.1038/NRN3469>.
41. Anderson, C.T., Sheets, P.L., Kiritani, T., and Shepherd, G.M.G. (2010). Sublayer-specific microcircuits of corticospinal and corticostriatal neurons in motor cortex. *Nat. Neurosci.* 13, 739–744. <https://doi.org/10.1038/NN.2538>.
42. von Nicolai, C., Engler, G., Sharott, A., Engel, A.K., Moll, C.K., and Siegel, M. (2014). Corticostriatal Coordination through Coherent Phase-Amplitude Coupling. *J. Neurosci.* 34, 5938–5948. <https://doi.org/10.1523/JNEUROSCI.5007-13.2014>.
43. Lemke, S.M., Ramanathan, D.S., Guo, L., Won, S.J., and Ganguly, K. (2019). Emergent Modular Neural Control Drives Coordinated Motor Actions. *Nat. Neurosci.* 22, 1122–1131. <https://doi.org/10.1038/S41593-019-0407-2>.
44. Joā Semedo, A.D., Zandvakili, A., Machens, C.K., Yu, B.M., Semedo, J.D., and Kohn, A. (2019). Cortical Areas Interact through a Communication Subspace. *Neuron* 102, 249–259.e4. <https://doi.org/10.1016/j.neuron.2019.01.026>.
45. Veuthey, T.L., Derosier, K., Kondapavulur, S., and Ganguly, K. (2020). Single-trial cross-area neural population dynamics during long-term skill learning. *Nat. Commun.* 11, 4057. <https://doi.org/10.1038/s41467-020-17902-1>.
46. Melzer, S., Gil, M., Koser, D.E., Michael, M., Huang, K.W., and Monyer, H. (2017). Distinct Corticostriatal GABAergic Neurons Modulate Striatal Output Neurons and Motor Activity. *Cell Rep.* 19, 1045–1055. <https://doi.org/10.1016/j.CELREP.2017.04.024>.
47. Kraft, A.W., Bauer, A.Q., Culver, J.P., and Lee, J.M. (2018). Sensory deprivation after focal ischemia in mice accelerates brain remapping and improves functional recovery through Arc-dependent synaptic plasticity. *Sci. Transl. Med.* 10, eaag1328. <https://doi.org/10.1126/scitranslmed.aag1328>.
48. Zeiler, S.R., Gibson, E.M., Hoesch, R.E., Li, M.Y., Worley, P.F., O'Brien, R.J., and Krakauer, J.W. (2013). Medial Premotor Cortex Shows a Reduction in Inhibitory Markers and Mediates Recovery in a Mouse Model of Focal Stroke. *Stroke* 44, 483–489. <https://doi.org/10.1161/STROKEAHA.112.676940>.
49. Otchy, T.M., Wolff, S.B.E., Rhee, J.Y., Pehlevan, C., Kawai, R., Kempf, A., Gobes, S.M.H., and Ölveczky, B.P. (2015). Acute off-target effects of neural circuit manipulations. *Nature* 528, 358–363. <https://doi.org/10.1038/nature16442>.
50. Zeiler, S.R., and Krakauer, J.W. (2013). The interaction between training and plasticity in the post-stroke brain. *Curr. Opin. Neurol.* 26, 609–616. <https://doi.org/10.1097/WCO.0000000000000025>.
51. Nudo, R.J., Plautz, E.J., and Frost, S.B. (2001). Role of adaptive plasticity in recovery of function after damage to motor cortex. *Muscle Nerve* 24, 1000–1019. <https://doi.org/10.1002/MUS.1104>.
52. Sanes, J.N., and Donoghue, J.P. (2000). Plasticity and primary motor cortex. *Annu. Rev. Neurosci.* 23, 393–415. <https://doi.org/10.1146/ANNUREV.NEURO.23.1.393>.
53. Plautz, E.J., Barbay, S., Frost, S.B., Stowe, A.M., Dancause, N., Zoubina, E.V., Eisner-Janowicz, I., Guggenmos, D.J., and Nudo, R.J. (2023). Spared premotor areas undergo rapid nonlinear changes in functional organization following a focal ischemic infarct in primary motor cortex of squirrel monkeys. *J. Neurosci.* 43, 2021–2032. <https://doi.org/10.1523/JNEUROSCI.1452-22.2023>.
54. Hu, J.J., Liu, Y., Yao, H., Cao, B., Liao, H., Yang, R., Chen, P., and Song, X.J. (2023). Emergence of consciousness from anesthesia through ubiquitin degradation of KCC2 in the ventral posteromedial nucleus of the thalamus. *Nat. Neurosci.* 26, 751–764. <https://doi.org/10.1038/s41593-023-01290-y>.
55. Belsey, P.P., Nicholas, M.A., and Yttri, E.A. (2020). Open-Source Joystick Manipulandum for Decision-Making, Reaching, and Motor Control Studies in Mice. *eNeuro* 7, ENEURO.0523-19.2020. <https://doi.org/10.1523/ENEURO.0523-19.2020>.
56. Santos, F.J., Oliveira, R.F., Jin, X., and Costa, R.M. (2015). Corticostriatal dynamics encode the refinement of specific behavioral variability during skill learning. *eLife* 4, e09423. <https://doi.org/10.7554/eLife.09423>.
57. Yin, H.H. (2014). Action, time and the basal ganglia. *Philos. Trans. R. Soc. Lond. B Biol. Sci.* 369, 20120473. <https://doi.org/10.1098/RSTB.2012.0473>.
58. Shadmehr, R., Reppert, T.R., Summerside, E.M., Yoon, T., and Ahmed, A.A. (2019). Movement vigor as a reflection of subjective economic utility. *Trends Neurosci.* 42, 323–336. <https://doi.org/10.1016/J.TINS.2019.02.003>.
59. Zeiler, S.R., Hubbard, R., Gibson, E.M., Zheng, T., Ng, K., O'Brien, R., and Krakauer, J.W. (2016). Paradoxical motor recovery from a first stroke after induction of a second stroke: re-opening a post-ischemic sensitive period. *Neurorehabil. Neural Repair* 30, 794–800. <https://doi.org/10.1177/1545968315624783>.
60. Guo, L., Kondapavulur, S., Lemke, S.M., Won, S.J., and Ganguly, K. (2021). Coordinated increase of reliable cortical and striatal ensemble activations during recovery after stroke. *Cell Rep.* 36, 109370. <https://doi.org/10.1016/j.celrep.2021.109370>.
61. Hooks, B.M., Papale, A.E., Paletzki, R.F., Feroze, M.W., Eastwood, B.S., Couey, J.J., Winnubst, J., Chandrashekhar, J., and Gerfen, C.R. (2018). Topographic precision in sensory and motor corticostriatal projections varies across cell type and cortical area. *Nat. Commun.* 9, 3549. <https://doi.org/10.1038/s41467-018-05780-7>.
62. Panigrahi, B., Martin, K.A., Li, Y., Graves, A.R., Vollmer, A., Olson, L., Mensh, B.D., Karpova, A.Y., and Dudman, J.T. (2015). Dopamine is required for the neural representation and control of movement vigor. *Cell* 162, 1418–1430. <https://doi.org/10.1016/j.cell.2015.08.014>.
63. Rueda-Orozco, P.E., and Robbe, D. (2015). The striatum multiplexes contextual and kinematic information to constrain motor habits execution. *Nat. Neurosci.* 18, 453–460. <https://doi.org/10.1038/nn.3924>.

64. Nelson, A.B., Bussert, T.G., Kreitzer, A.C., and Seal, R.P. (2014). Striatal cholinergic neurotransmission requires VGLUT3. *J. Neurosci.* 34, 8772–8777. <https://doi.org/10.1523/JNEUROSCI.0901-14.2014>.
65. Roberts, B.M., White, M.G., Patton, M.H., Chen, R., and Mathur, B.N. (2019). Ensemble encoding of action speed by striatal fast-spiking interneurons. *Brain Struct. Funct.* 224, 2567–2576. <https://doi.org/10.1007/S00429-019-01908-7>.
66. Plenz, D. (2003). When inhibition goes incognito: feedback interaction between spiny projection neurons in striatal function. *Trends Neurosci.* 26, 436–443. [https://doi.org/10.1016/S0166-2236\(03\)00196-6](https://doi.org/10.1016/S0166-2236(03)00196-6).
67. Gage, G.J., Stoetzner, C.R., Wiltschko, A.B., and Berke, J.D. (2010). Selective activation of striatal fast-spiking interneurons during choice execution. *Neuron* 67, 466–479. <https://doi.org/10.1016/J.NEURON.2010.06.034>.
68. Gittis, A.H., Nelson, A.B., Thwin, M.T., Palop, J.J., and Kreitzer, A.C. (2010). Distinct roles of GABAergic interneurons in the regulation of striatal output pathways. *J. Neurosci.* 30, 2223–2234. <https://doi.org/10.1523/JNEUROSCI.4870-09.2010>.
69. Mallet, N., Le Moine, C., Charpier, S., and Gonon, F. (2005). Feedforward inhibition of projection neurons by fast-spiking GABA interneurons in the rat striatum *in vivo*. *J. Neurosci.* 25, 3857–3869. <https://doi.org/10.1523/JNEUROSCI.5027-04.2005>.
70. Berke, J.D. (2011). Functional properties of striatal fast-spiking interneurons. *Front. Syst. Neurosci.* 5, 45. <https://doi.org/10.3389/FNSYS.2011.00045>.
71. Lee, K., Holley, S.M., Shobe, J.L., Chong, N.C., Cepeda, C., Levine, M.S., and Masmanidis, S.C. (2017). Parvalbumin Interneurons Modulate Striatal Output and Enhance Performance during Associative Learning. *Neuron* 93, 1451–1463.e4. <https://doi.org/10.1016/J.NEURON.2017.02.033>.
72. Johansson, Y., and Silberberg, G. (2020). The Functional Organization of Cortical and Thalamic Inputs onto Five Types of Striatal Neurons Is Determined by Source and Target Cell Identities. *Cell Rep.* 30, 1178–1194.e3. <https://doi.org/10.1016/J.CELREP.2019.12.095>.
73. Ramanathan, S., Hanley, J.J., Deniau, J.M., and Bolam, J.P. (2002). Synaptic Convergence of Motor and Somatosensory Cortical Afferents onto GABAergic Interneurons in the Rat Striatum. *J. Neurosci.* 22, 8158–8169. <https://doi.org/10.1523/JNEUROSCI.22-18-08158.2002>.
74. Desmurget, M., and Turner, R.S. (2010). Motor sequences and the basal ganglia: Kinematics, not habits. *J. Neurosci.* 30, 7685–7690. <https://doi.org/10.1523/JNEUROSCI.0163-10.2010>.
75. Bauer, A.Q., Kraft, A.W., Wright, P.W., Snyder, A.Z., Lee, J.M., and Culver, J.P. (2014). Optical imaging of disrupted functional connectivity following ischemic stroke in mice. *Neuroimage* 99, 388–401. <https://doi.org/10.1016/J.NEUROIMAGE.2014.05.051>.
76. von Monakow, C. (1914). *Die Lokalisation im Grosshirn und der Abbau der Funktion durch kortikale Herde* (Wiesbaden: J.F. Bergmann).
77. Gharabawie, O.A., and Whishaw, I.Q. (2006). Parallel stages of learning and recovery of skilled reaching after motor cortex stroke: “oppositions” organize normal and compensatory movements. *Behav. Brain Res.* 175, 249–262. <https://doi.org/10.1016/J.BBR.2006.08.039>.
78. Hong, Y.K., Lacefield, C.O., Rodgers, C.C., and Bruno, R.M. (2018). Sensation Movement and Learning in the Absence of Barrel Cortex. *Nature* 561, 542–546. <https://doi.org/10.1038/S41586-018-0527-Y>.
79. Hwang, E.J., Dahlen, J.E., Mukundan, M., and Komiyama, T. (2017). History-based action selection bias in posterior parietal cortex. *Nat. Commun.* 8, 1242. <https://doi.org/10.1038/s41467-017-01356-z>.
80. Hwang, E.J., Link, T.D., Hu, Y.Y., Lu, S., Wang, E.H.J., Lilascharoen, V., Aronson, S., O’Neil, K., Lim, B.K., and Komiyama, T. (2019). Corticostratial Flow of Action Selection Bias. *Neuron* 104, 1126–1140.e6. <https://doi.org/10.1016/J.NEURON.2019.09.028>.
81. Mooshagian, E., Yttri, E.A., Loewy, A.D., and Snyder, L.H. (2022). Contralateral Limb Specificity for Movement Preparation in the Parietal Reach Region. *J. Neurosci.* 42, 1692–1701. <https://doi.org/10.1523/JNEUROSCI.0232-21.2021>.
82. Yttri, E.A., Wang, C., Liu, Y., and Snyder, L.H. (2014). The parietal reach region is limb specific and not involved in eye-hand coordination. *J. Neurophysiol.* 111, 520–532. <https://doi.org/10.1152/jn.00058.2013>.
83. Hanks, T.D., Kopec, C.D., Brunton, B.W., Duan, C.A., Erlich, J.C., and Brody, C.D. (2015). Distinct relationships of parietal and prefrontal cortices to evidence accumulation. *Nature* 520, 220–223. <https://doi.org/10.1038/nature14066>.
84. Ginis, P., Nackaerts, E., Nieuwboer, A., and Heremans, E. (2018). Cueing for people with Parkinson’s disease with freezing of gait: A narrative review of the state-of-the-art and novel perspectives. *Ann. Phys. Rehabil. Med.* 61, 407–413. <https://doi.org/10.1016/J.REHAB.2017.08.002>.
85. Farr, T.D., and Whishaw, I.Q. (2002). Quantitative and Qualitative Impairments in Skilled Reaching in the Mouse (*Mus musculus*) After a Focal Motor Cortex Stroke. *Stroke* 33, 1869–1875. <https://doi.org/10.1161/01.STR.0000020714.48349.4E>.
86. Miri, A., Warriner, C.L., Seely, J.S., Elsayed, G.F., Cunningham, J.P., Churchland, M.M., and Jessell, T.M. (2017). Behaviorally Selective Engagement of Short-Latency Effector Pathways by Motor Cortex. *Neuron* 95, 683–696.e11. <https://doi.org/10.1016/j.neuron.2017.06.042>.
87. Passingham, R.E., Perry, V.H., and Wilkinson, F. (1983). The long-term effects of removal of sensorimotor cortex in infant and adult rhesus monkeys. *Brain* 106, 675–705. <https://doi.org/10.1093/BRAIN/106.3.675>.
88. Martin, J.H., and Ghez, C. (1993). Differential impairments in reaching and grasping produced by local inactivation within the forelimb representation of the motor cortex in the cat. *Exp. Brain Res.* 94, 429–443. <https://doi.org/10.1007/BF00230201>.
89. Shadmehr, R., and Krakauer, J.W. (2008). A COMPUTATIONAL NEUROANATOMY FOR MOTOR CONTROL. *Exp. Brain Res.* 185, 359–381. <https://doi.org/10.1007/S00221-008-1280-5>.
90. Nudo, R.J., and Friel, K.M. (1999). Cortical plasticity after stroke: implications for rehabilitation. *Rev. Neurol. (Paris)* 155, 713–717.
91. Biernaskie, J., Szymanska, A., Windle, V., and Corbett, D. (2005). Bihemispheric contribution to functional motor recovery of the affected forelimb following focal ischemic brain injury in rats. *Eur. J. Neurosci.* 21, 989–999. <https://doi.org/10.1111/J.1460-9568.2005.03899.X>.
92. Gharabawie, O.A., Karl, J.M., and Whishaw, I.Q. (2007). Recovery of skilled reaching following motor cortex stroke: do residual corticofugal fibers mediate compensatory recovery? *Eur. J. Neurosci.* 26, 3309–3327. <https://doi.org/10.1111/J.1460-9568.2007.05874.X>.
93. Hakon, J., Quattrone, M.J., Sjölund, C., Tomasevic, G., Carey, L., Lee, J.M., Ruscher, K., Wieloch, T., and Bauer, A.Q. (2018). Multisensory stimulation improves functional recovery and resting-state functional connectivity in the mouse brain after stroke. *NeuroImage Clin.* 17, 717–730. <https://doi.org/10.1016/J.NICL.2017.11.022>.
94. Mizes, K.G.C., Lindsey, J., Escola, G.S., and Ölveczky, B.P. (2023). Dissociating the contributions of sensorimotor striatum to automatic and visually guided motor sequences. *Nat. Neurosci.* 26, 1791–1804. <https://doi.org/10.1038/s41593-023-01431-3>.
95. Gadagkar, V., Puzerey, P.A., Chen, R., Baird-Daniel, E., Farhang, A.R., and Goldberg, J.H. (2016). Dopamine neurons encode performance error in singing birds. *Science* 354, 1278–1282. <https://doi.org/10.1126/SCIENCE.AAH6837>.
96. Arber, S., and Costa, R.M. (2018). Connecting neuronal circuits for movement. *Science* 360, 1403–1404. <https://doi.org/10.1126/SCIENCE.AAT5994>.
97. Sobinov, A.R., and Bensmaia, S.J. (2021). The neural mechanisms of manual dexterity. *Nat. Rev. Neurosci.* 22, 741–757. <https://doi.org/10.1038/s41583-021-00528-7>.
98. Cowie, D., Limousin, P., Peters, A., Hariz, M., and Day, B.L. (2012). Doorway-provoked freezing of gait in Parkinson’s disease. *Mov. Disord.* 27, 492–499. <https://doi.org/10.1002/MDS.23990>.

99. Miranda-Domínguez, Ó., Ragothaman, A., Hermosillo, R., Feczko, E., Morris, R., Carlson-Kuhta, P., Nutt, J.G., Mancini, M., Fair, D., and Horak, F.B. (2020). Lateralized Connectivity between Globus Pallidus and Motor Cortex is Associated with Freezing of Gait in Parkinson's Disease. *Neuroscience* 443, 44–58. <https://doi.org/10.1016/J.NEUROSCIENCE.2020.06.036>.
100. Topka, M., Schneider, M., Zrenner, C., Belardinelli, P., Ziemann, U., and Weiss, D. (2022). Motor cortex excitability is reduced during freezing of upper limb movement in Parkinson's disease. *NPJ Parkinsons Dis* 8, 161. <https://doi.org/10.1038/s41531-022-00420-w>.
101. Dagan, M., Herman, T., Harrison, R., Zhou, J., Giladi, N., Ruffini, G., Manor, B., and Hausdorff, J.M. (2018). Multitarget transcranial direct current stimulation for freezing of gait in Parkinson's disease. *Mov. Disord.* 33, 642–646. <https://doi.org/10.1002/MDS.27300>.
102. Cheng, H.W., Tong, J., and McNeill, T.H. (1998). Lesion-induced axon sprouting in the deafferented striatum of adult rat. *Neurosci. Lett.* 242, 69–72. [https://doi.org/10.1016/S0304-3940\(98\)00050-0](https://doi.org/10.1016/S0304-3940(98)00050-0).
103. Jun, J.J., Mitelut, C., Lai, C., Gratiy, S.L., Anastassiou, C.A., and Harris, T.D. (2017). Real-time spike sorting platform for high-density extracellular probes with ground-truth validation and drift correction. Preprint at bioRxiv, 101030.
104. Tennant, K.A., Adkins, D.L., Donlan, N.A., Asay, A.L., Thomas, N., Kleim, J.A., and Jones, T.A. (2011). The organization of the forelimb representation of the C57BL/6 mouse motor cortex as defined by intracortical microstimulation and cytoarchitecture. *Cereb. Cortex* 21, 865–876. <https://doi.org/10.1093/cercor/bhq159>.
105. Peters, A.J., Fabre, J.M.J., Steinmetz, N.A., Harris, K.D., and Carandini, M. (2021). Striatal activity topographically reflects cortical activity. *Nature* 591, 420–425. <https://doi.org/10.1038/s41586-020-03166-8>.
106. Yamin, H.G., Stern, E.A., and Cohen, D. (2013). Parallel processing of environmental recognition and locomotion in the mouse striatum. *J. Neurosci.* 33, 473–484. <https://doi.org/10.1523/JNEUROSCI.4474-12.2013>.
107. Schmitzer-Torbert, N.C., and Redish, A.D. (2008). Task-dependent encoding of space and events by striatal neurons is dependent on neural subtype. *Neuroscience* 153, 349–360. <https://doi.org/10.1016/J.NEUROSCIENCE.2008.01.081>.

STAR★METHODS

KEY RESOURCES TABLE

REAGENT or RESOURCE	SOURCE	IDENTIFIER
Experimental models: Organisms/strains		
Mouse: C57Bl/6J	The Jackson Laboratory	#000664
Software and algorithms		
MATLAB 2017b	MathWorks	RRID:SCR_001622
JRClust v3	Jun et al. ¹⁰³	https://github.com/JaneliaSciComp/JRCLUST
SpikeGLX	Janelia Research Campus	https://github.com/billkarsh/SpikeGLX
Inkscape 0.92.4	Inkscape	RRID:SCR_014479
Analysis software	This paper	https://doi.org/10.5281/zenodo.12812626
Other		
Joystick behavior rig	Belsey et al. ⁵⁵	https://github.com/YttriLab/Joystick

RESOURCE AVAILABILITY

Lead contact

Further information and requests for resources should be directed to and will be fulfilled by the lead contact, Eric A. Yttri (eyttri@andrew.cmu.edu).

Materials availability

This study did not generate new unique reagents.

Data and code availability

- All data reported in this paper will be shared by the [lead contact](#) upon request.
- All original code has been deposited at Zenodo and is publicly available as of the date of publication. The DOI is listed in the [key resources table](#).
- Any additional information required to reanalyze the data reported in this paper is available from the [lead contact](#) upon request

EXPERIMENTAL MODEL AND STUDY PARTICIPANT DETAILS

Adult C57Bl6 mice (The Jackson Laboratory, #000664) were used in these experiments, four for the basic reaching task (two females), four for the cued reaching task (two females) which both received bilateral M1 lesions. Four additional mice were trained on the basic reaching task (one female) and received bilateral PPC lesions. Animals run on the cued response task were also used for the T-maze task, and were compared to a control group of five unlesioned adult mice (three females) that had also undergone joystick training for an unrelated project. Mouse health and weight were monitored daily and water intake was controlled to 1-1.5 ml water per day. Mice were pair-housed when possible and held in a temperature and humidity controlled room maintained on a reversed 12 hour light/dark cycle. While sex was counterbalanced, no sex based differences were tested potentially limiting this study's generalizability. All experiments and procedures were approved by the Carnegie Mellon University Institutional Animal Care and Use Committee.

METHOD DETAILS

Joystick tasks

Behavioral sessions occurred at the same time of day Pre and Post lesion. Sessions in the basic task normally lasted 30 minutes and sessions in the cued joystick task normally lasted 40 minutes (session length based on average amount of time to get roughly 1 cc of water). Following lesion, if an animal performed less than 15 reaches in 20 minutes the session was ended.

Mice were trained using the software and hardware as previously described.⁵⁵ Training sessions occurred once per day after the initial week of acclimation training, in which two sessions occurred. Mice were trained on one of two tasks; the basic, self-paced reaching task and the cued joystick task. Both tasks were performed in a darkened chamber using a spring loaded, Hall effect joystick

(Ruffy Controls, Miniature 2 axis hall effect joystick TS1-1-R-R-1-BK) mounted roughly 2 cm below the mouse's eyes while head fixed. The joysticks require 0.18 N for displacement. Hall effect joysticks use a single, central spring, and therefore applies a uniform resistance in any direction. Movements greater than 0.9 cm in any direction - left, right, forwards, backwards - from joystick center resulted in a reward when performed at the correct time in the task. Rewards were delivered via a lick port positioned directly in front of the mouth. Behavioral data was recorded using an Arduino Mega, sampling joystick position at 16 Hz. Code for data collection, reach detection, and offline analysis can be found at <https://github.com/YttriLab/Joystick>.

In the self-paced, basic reaching task, mice learned to displace a joystick past a threshold (0.9 cm) to gain a sweetened water reward (0.3 mM acesulfame potassium) after a delay of 1 second, which was signaled by an audible click of the solenoid controlling water flow. The reward was delayed to dissociate movement and reward-related activity. An inter-trial interval (ITI) of 3 seconds followed reward delivery, during which no joystick movements would be rewarded, and typically no movements occurred during this time. No cue was given to signal the end of this ITI.

The cued response, center out reaching task differed in that rewarded joystick movements must follow the onset of a white cue LED positioned 1-2 cm in front of the mouse's right eye. This task provides the opportunity to assess both the temporal component of the performance and the effects of a cue. In a successful trial, moving the joystick past the threshold (0.9 cm) would immediately turn off the cue light and result in a sweetened water reward after the same 1 second delay. After reward delivery, a random ITI was selected from a uniform distribution of 5 to 10 seconds. During the last 20% of the ITI, any joystick movement with an amplitude exceeding the reward threshold resulted in a timeout in which house lights would turn on for 5 seconds. Following this punishment timeout, the house lights would turn off and a new random ITI was executed. Movements before this period were not punished and were considered as unrewarded. Response time was defined as the time between the cue light turning on and reach initiation. Response times greater than 2000 ms were considered to be well beyond the delay with which an animal would respond to a cue. Response times under 50 ms were rare, and were deemed to be preemptive rather than responsive. All reaches were included in our analyses except when identified as "Responsive Reaches", e.g. [Figure 2H](#). We observed no kinematic differences for reaches falling inside or outside of this distinction.

While only reaches surpassing an amplitude 0.9 cm were rewarded, reach amplitudes as small as 0.05 cm were reliably detected in offline analysis. All reaches above this 0.05 cm baseline detected offline, rewarded and rewarded reaches, were used in these behavioral analyses.

Upon the conclusion of M1 lesion data collection, we noted that the deficits incurred in the self-paced and cued reaching were analogous. The inclusion of PPC lesions aimed to contrast the contribution of different cortical areas, and in particular, to control for off-target effects of lesioning - such as diaschisis. Because of this objective, we opted for the uncued version of the task to remove the confound of the mouse having altered visual perception after a lesion to this visuomotor area.

Experimental setup

One week after surgical implantation of a head fixation cap, mice were handled, acclimated to head fixation, and transitioned to a controlled watering schedule. Mice were trained in the same behavioral training rig on either version of the task over the course of 5-7 weeks (44.9 ± 4.4 sessions, mean \pm SEM) to get to expert performance as previously described.⁵⁵ Mice that were to be recorded from were then transitioned to an identical joystick rig with electrophysiological recording capabilities. After a week of acclimating to the new behavioral rig, we performed a craniotomy centered over the left CFA - left striatum. Several hours later, the mouse performed its first Pre session. After at least three Pre recording sessions, the mouse received bilateral aspiration lesions in the morning. The mouse then performed the first session in Post 1 (roughly 4 hours later) on the same day. Mice in the basic uncued reach task were not recorded from and continued to perform post lesion experimental sessions using the same joystick rig in which they trained throughout the entire experiment. When possible mice were run for a total of 20 days post lesion. Of the four mice used for electrophysiological recordings, the minimum number of sessions post lesion (including the day of the lesion) was 14 and the maximum number of sessions was 19.

Surgical procedures

Before training, each mouse was surgically implanted under aseptic conditions with a head fixation cap (<https://github.com/YttriLab/Joystick/blob/master/Mouse%20Shuttle%20Parts/Headcap>, SLDPR) while under isoflurane anesthesia (1.5-2.0%). The head fixation cap was placed parallel to the skull leveled relative to bregma and lambda, with visual access to the bregmatic suture and marked lesion and recording coordinates maintained through a layer of clear dental cement. Mice were carefully monitored after surgery and given carprofen (5 mg/kg) as a post-operative analgesic for two days.

To lesion the caudal forelimb area, mice were head fixed and anesthetized using isoflurane (1.5-2.0%) and the dental cement above the CFA was cleared above the skull. A small bone flap was removed, spanning laterally from bregma 0.5 to 2.5 mm and anteriorly 1.5 to 1.5 mm, revealing CFA as described in Tennant et al.¹⁰⁴ The exposed cortical tissue was removed using a 20 gauge Rosen suction tube until tissue lightened in color, signaling the proximity to corpus callosum. This procedure was performed bilaterally. Control bilateral lesions to posterior parietal cortex were performed in the same manner as described above, centered on the following coordinates: 2.2 to 3.12 mm lateral and -1.9 to -2.1 mm posterior relative to bregma. Surrounding tissue was removed to match the M1 lesion volume.

Unrewarded T-maze task

Mice that were run on the cued response joystick task participated in a simple, unrewarded T-maze task. This task provides a complimentary assessment of non-dexterous, non-goal oriented behavior. A trial consisted of the mouse being placed at the base of the T (center hallway width: 8 cm, length: 50 cm, crossing hallway width: 8 cm, length: 35 cm) facing the T-junction. It was then allowed to navigate freely. This was done five times per session, starting from the base of the T. Testing began the day before lesion and continued for 15 sessions. Video was recorded from above at 30 fps. Mouse position was calculated offline using custom blob detection software written in MATLAB.

Electrophysiology data acquisition

To assay striatal activity, we acutely recorded dorsal striatal activity from at approximately 0.5 mm anterior, 1.8 mm lateral of bregma using a 64-channel silicon electrode spanning 2.1 to 2.9 mm (2 shanks with 32 channels each, Cambridge Neurotechnology) or 2.45 to 2.85 mm (4 shanks with 16 channels each, Cambridge Neurotechnology) from the surface of the brain using aseptic conditions (Figure S10). As discussed in the text, this area has been shown to receive dense projections from CFA and rostral forelimb area of mouse M1, as well as other areas⁶¹; also see Extended Figure 1 of Yttri and Dudman³⁵ for retrobead targeted dorsal striatum results identifying projections from CFA. Signals were sampled at 25 kHz with a Whisper data acquisition system (Neural Circuits, LLC) running SpikeGLX software (<https://github.com/billkarsh/SpikeGLX>). Spiking activity was then band-pass filtered (300 Hz-3 kHz) and sorted offline using open-source software (JRClust,¹⁰³ <https://github.com/JaneliaSciComp/JRCLUST>).

Histology

Following experimentation animals were euthanized and perfused with chilled 4% paraformaldehyde and then tissue was placed in a 30% sucrose solution. The brain was then sectioned in 50 μ m slices and stained with DAPI mounting media (Abcam, ab104139). Histological verification of lesion location and extent was confirmed by outlining lesion boundaries with the use of matched atlas section (Paxinos) and surgical notes. Lesion overlap maps from this information were generated using custom software.

QUANTIFICATION AND STATISTICAL ANALYSIS

Joystick kinematics analysis

Reach trajectories and kinematics were isolated and quantified as previously described.⁵⁵ Normalized trajectory SEM was determined by first rotating every reach such that its peak amplitude progressed along the X axis. We then warped the X and Y dimensions of every reach by this peak amplitude value, such that the start of every reach began at the origin (0,0) and the furthest extent was located at (1,0). Reaches with greater deviation from the central axis of the reach trajectory would thus have greater Y values. This was done to better compare across reaching movements of considerably different amplitudes. We then plotted the SEM of these Y values across multiple points along the outward reaching component (X axis).

Striatal cell identification

Striatal cell identity was determined using a combination of waveform characteristics and spike timing similar to previous studies.^{105,106} Each single unit was upsampled from 25 kHz to 250 kHz using spline fitting (MATLAB). Peak-to-trough time, proportion of long interspike-intervals (ISIs) and post spike suppression were used to determine neuron identity. The proportion of long ISIs was calculated for each neuron by summing all ISIs which exceeded 2 seconds and dividing by the total recording time.¹⁰⁷ Post spike suppression was calculated by finding the time a neuron's firing rate was suppressed following an action potential. For each neuron the sum of the number of 1 ms bins of its autocorrelation function below the average firing rate between the 600 to 900 ms autocorrelation bins was considered its post spike suppression.¹⁰⁵ Units with peak-to-trough time of less than 350 μ s and a proportion long inter-spike-interval less than 10% were considered putative FSIs while units with a proportion long ITI greater than 10% and peak-to-trough time of less than 350 μ s were considered unidentified interneurons. Units with peak-to-trough time of greater than 350 μ s and post spike suppression less than 40 ms were considered putative SPNs.

Less than 1% of identified units exhibited a post spike suppression greater than 40 ms and a peak-to-trough greater than 350 μ s. These units were considered tonically active neurons (TANs) and along with the unidentified interneurons and any units with an average firing rate less than 0.1 Hz were excluded from further analysis, see Figure S3.

Electrophysiology data analysis

Single unit and behavioral data analyses were performed using custom-written software in Matlab. Spikes of isolated single units were counted within 20 ms bins to generate the average response per unit aligned to reach start. Z-score normalization used the mean and standard deviation of each neuron's firing rate during the period from 3 seconds before reach onset to 2 seconds before reach onset. Percent of reach-modulated neurons was determined using a rank sum test between each neuron's same baseline

period and -200 to 600 ms around reach onset similar to other mouse joystick studies.⁶² To create a null distribution for bootstrapping, we repeated this 1000 times for each recording session, but with each iteration using random reach start times, keeping the number of trials the same. The 99% confidence interval was found for each analysis epoch and compared to the experimental data when applicable. To determine if there was a post-lesion change in the proportion of significantly reach-modulated neurons from that found in Pre, we used a random subset of trials equal to the mean reach count in each Post epoch (3, 17, 81, or 100 trials for Post 1-4, respectively). For each neuron in Pre, we selected 17 trials at random from the session that neuron was recorded from. We then computed the significance of the reach responsivity using only those 17 trials. This was repeated for 1,000 iterations per neuron. We used the mean p-value across these 1,000 iterations to determine whether it was reach modulated. After doing this for every Pre neuron, the resulting proportion of significant modulated neurons was used for comparison with the respective Post lesion block. Unlike suprethreshold reaches, small forelimb movements in Post 2-4 had similar or greater mean counts to Pre (Pre = 48, Post 1 = 20, Post 2 = 33, Post 3 = 93, Post 4 = 97).

To determine whether a neurons activity is modulated by reach amplitude, we calculated an amplitude modulation index. This index is the difference between the mean absolute Z-scored activity of a neuron during large (>0.9 cm) and small (<0.5 cm) reaches over the period of -200 to 600 ms relative to reach initiation. For example, if a neuron is equally responsive to both large and small reaches, the index value would be equal to zero; if it is two z-scores more active for large reaches, the index value would be positive two. We quantify the neural-behavioral relationship this way because of the range of amplitudes across different post-lesion epochs. In early post-lesion sessions, the overwhelming majority of reach amplitudes are within a tight and narrow range (see trial-by-trial histogram, [Figure 2I](#)). Additionally, measures like Pearson correlation assume a linear relationship, which may or may not be the case and is difficult to quantify given SPNs characteristic lower firing rates. This index makes no assumption of linearity of amplitude tuning. As a note, the mean session amplitude in [Figures 3E](#) and [4E](#) is calculated with the requirement that neurons were recorded in a given session during both reaches greater than 0.9 cm and less than 0.5 cm. Thus, exclusion of a session owing to this recording requirement may slightly alter the mean amplitude value on the y axis.

Joystick decoding from striatal activity

For Pre and each Post lesion epoch, a feedforward neural network was used to predict joystick position from neural activity recorded in the striatum. The network was built using the MATLAB *feedforwardnet* function and contained 3 hidden layers with 10 units each. Joystick position and accompanying neural data -499 to 1000 ms relative to the start of each reach and binned at 100 ms. These bounds were selected to include preparatory activity and the full duration of the reach (mean and standard deviation duration across sessions = 717.9 ± 391.3 ms). Reaches that were less than 0.45 cm were excluded from analysis. Sessions with less than five reaches total were excluded, thus the absence of Post 1 data. Neural spike counts per bin were smoothed using a Gaussian-weighted moving average over each window of 4 time bins and served as the input data. To enable more input-target observations to train and test the model, and thus a more accurate account of the reach-related information carried by this population, we concatenated all reaches and their relative neural activity across a given post-lesion epoch. In this multivariate input, the neural activity in a given time bin is still mapped to the respective joystick amplitude. Post 2 had the smallest reach count for any epoch, yielding 132 reaches meeting our criterion and thus 1980 observations (per-neuron spike count and amplitude tuples). To ensure the same number of training and testing observations regardless of epoch, we randomly subsampled 132 reaches from each epoch's concatenated datasets. Doing so enables a balanced comparison between all Pre and Post lesion epochs. To compensate for the different numbers of neurons recorded in each session, a random selection of 10 neurons was used for each reach. This random selection of neurons was repeated 10 times for each set of 132 reaches. The model trained and tested anew each time, and the mean performance was calculated as the average across the 10 repeats for a given set of joystick amplitudes. A random 70% of the 1980 observations was used for training while 15% was used for validation and the remaining 15% was used for testing. The model was limited to 750 training epochs using Bayesian regularization. This process was repeated 50 times (500 iterations total per epoch), and the 50 mean normalized MSEs from each epoch are plotted in [Figure 5](#). This analysis was repeated using 30 neurons in [Figure S8](#).

The variability of reach amplitudes in [Figure 5C](#) was computed using the Coefficient of Dispersion, also sometimes called the Quartile Coefficient of Dispersion or QCD. The Coefficient of Dispersion is simply a contrast ratio of the inter-quartile ranges, e.g. $(Q3-Q1)/(Q3+Q1)$. This method is similar to Coefficient of Variation, but makes no such assumptions about normalcy or scale of the datasets. As the scale of amplitudes varied greatly between epochs, with median values spanning an order of magnitude, we found this method to be the most appropriate.

T-Maze analysis

To analyze T-maze videos, the maze was partitioned into 5 cm-long segments. These segments were numbered from 1 at the base to 10 at the intersection of the hallways, then labeled 11 to 13 in both directions moving away from the junction. There were no markers for this in the actual T-maze. Occupancy values were determined by counting the number of frames (recorded at 30 fps) the center of the mouse body was found to occupy each portion of the T-maze. Locomotor speed was not used because this would fail to capture the prolonged duration of immobility at the junction, although average speed along a hallway can be roughly determined by dividing the time per division by the length of the division (5 cm).

Statistical testing

The number of animals and sessions used were based upon previous mouse lesion and joystick studies using an intersession, within-animal control model. Experimenters were not blinded to lesion condition. Statistical tests are reported in the respective figure legends and in the results text. Statistical testing was done at the session level as described in the main text. To determine if lesions of M1 or PPC affected mice differently, task performance, reach kinematic and amplitude modulation was analyzed using mixed-effects ANOVAs. Each variable of interest (inter-reach interval, amplitude, peak speed ect.) served as a dependent variable in separate analyses. Factors included mouse (1-4), lesion (pre, post) and session (pre-lesion day -5 to post lesions 19, continuous) with lesion nested under mouse.

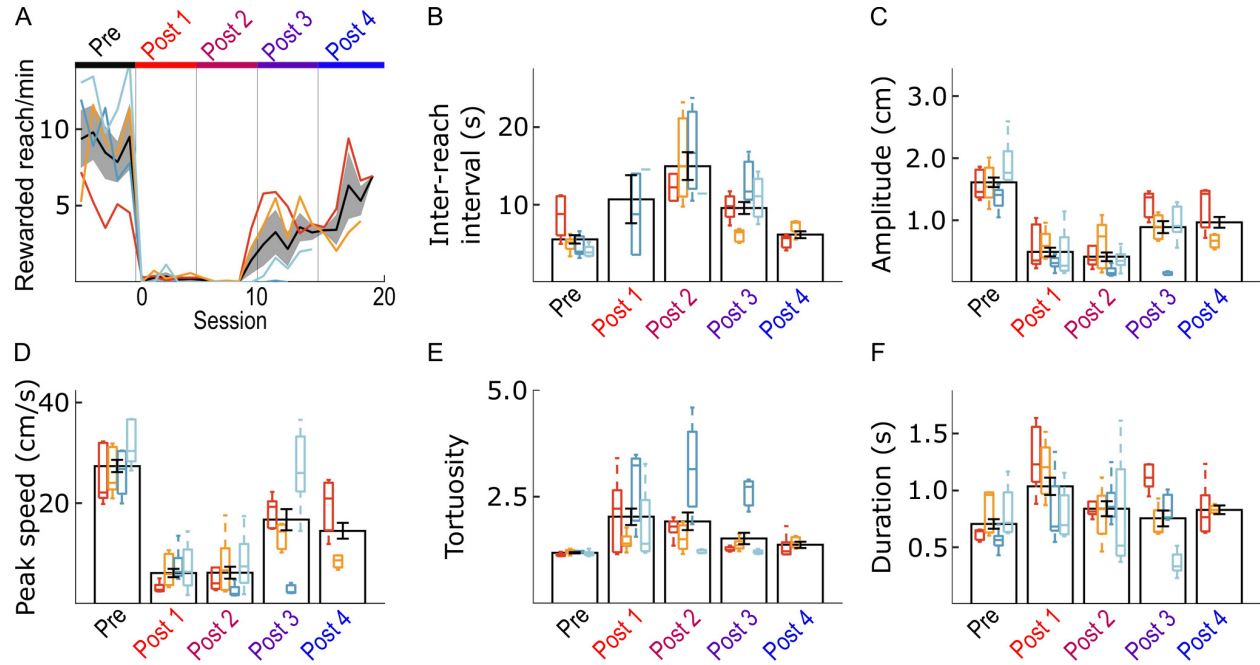
Supplemental information

Motor cortex is responsible for motoric dynamics in striatum and the execution of both skilled and unskilled actions

Mark A. Nicholas and Eric A. Yttri

Supplemental Information

Supplemental Figure 1



Supplemental Figure 1. Individual animal performance and kinematics during the basic reaching task, related to Figure 2.

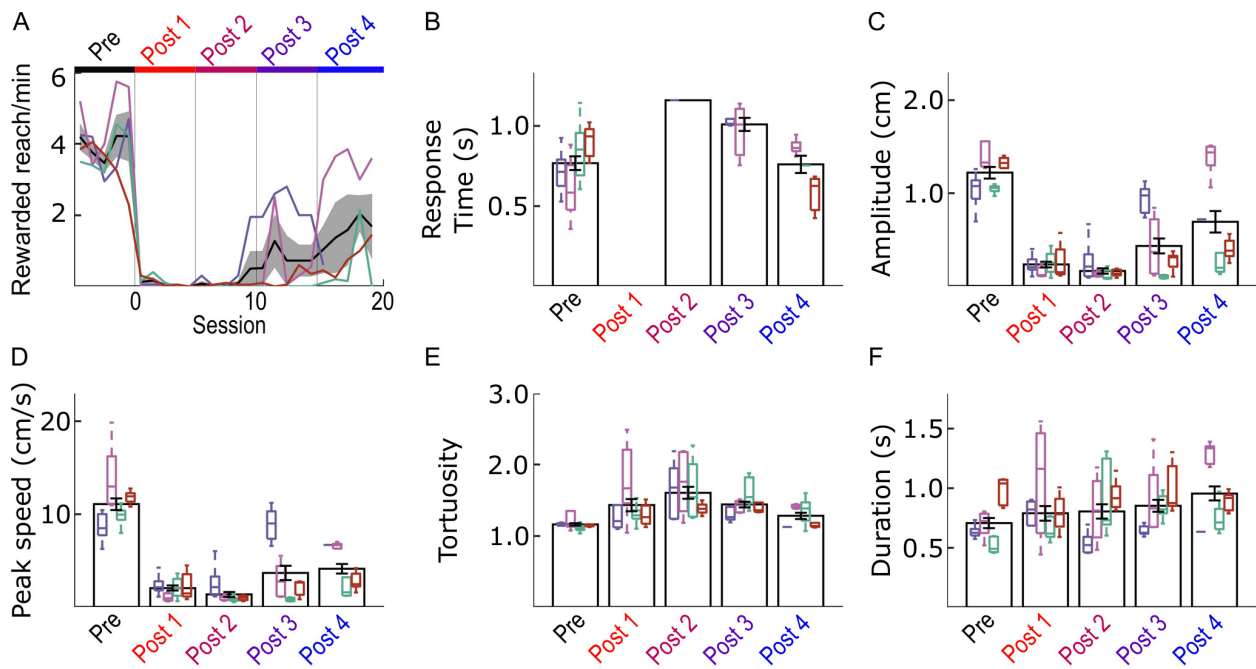
(A) Mean rewarded reach rate over the first 20 minutes of each session relative to the day of lesion (mean \pm SEM) for mice run on the basic reaching task ($n = 4$). Individual animals are plotted and colors are preserved for each animal throughout all panels. To determine if the lesion had differing effects of task performance and kinematics for mice differently, we ran independent mixed-effects ANOVAs for each variable of interest (see methods for further details). We found a main effect of lesion for the rewarded trial rate ($F(4,86) = 40.0$, $P = 2.39 \times 10^{-17}$) however it also varied function of mouse ($F(3,86) = 9.29$, $P = 2.94 \times 10^{-5}$) which suggests that mice may solve the task in various ways while all being effected by the lesion.

(B) Average inter-reach interval did not vary as a function of mouse ($F(3,85) = 0.73$, $P = 0.54$).

(C) Reach amplitude did have a main effect of mouse ($F(3,70) = 3.74$, $P = 0.015$) however there was no interaction of lesion and session ($F(4,70) = 1.87$, $P = 0.13$) suggesting that even though the mice are

different, the deficit and recovery of reach amplitude did not vary as a function of the lesion with respect to session number, that is, the effect of lesion and recovery over time was similar across mice. We found no main effect of mouse for (D) peak speed ($F(3,70) = 1.87$, $P = 0.14$), (E) tortuosity ($F(3,85) = 0.98$, $P = 0.41$) nor (F) duration ($F(3,70) = 0.71$, $P = 0.55$). The mouse depicted by red performed 40 sessions prior to lesion. The mouse depicted by gold performed 38 sessions prior to lesion. The mouse depicted by the darker blue performed 45 sessions prior to lesion. The mouse depicted by the lighter blue performed 42 sessions prior to lesion.

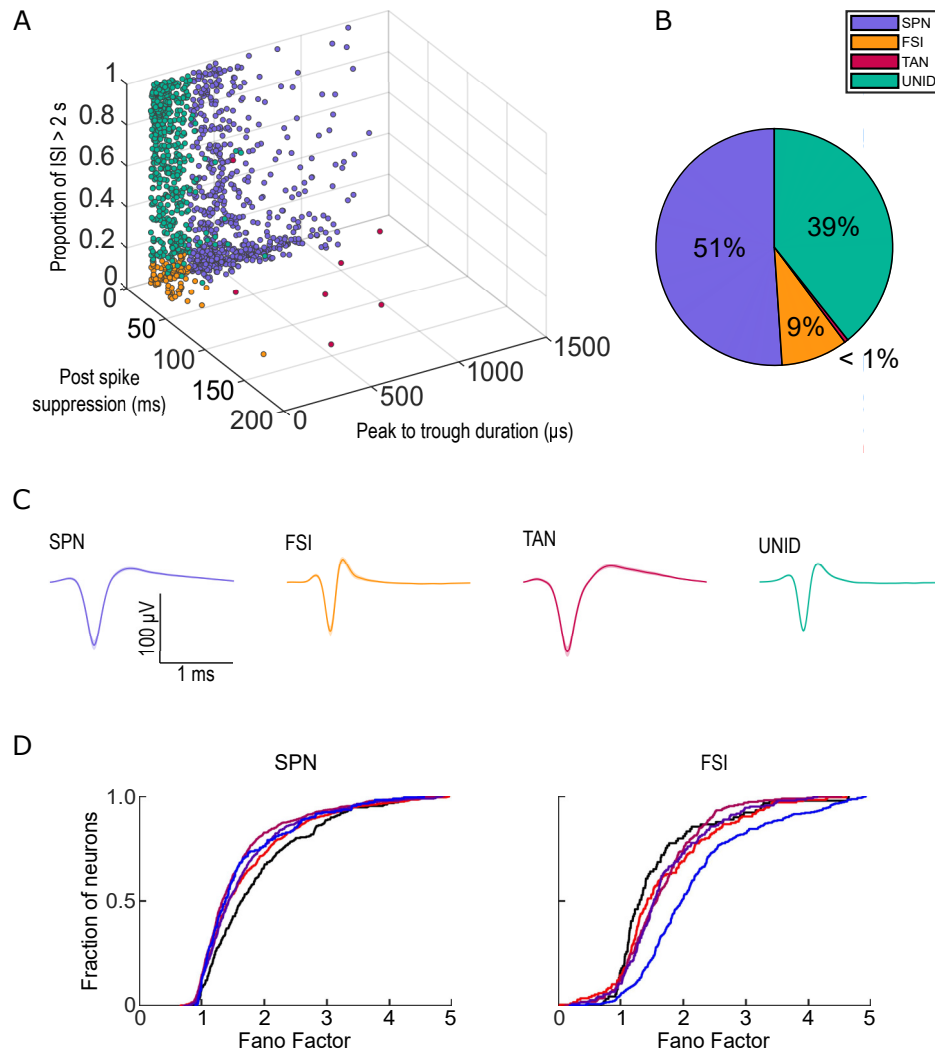
Supplemental Figure 2



Supplemental Figure 2. Individual animal performance and kinematics during the cued response reaching task, related to Figure 2.

(A) Mean rewarded reach rate over the first 20 minutes of each session relative to the day of lesion (mean \pm SEM) for mice run on the cued response reaching task ($n = 4$). Individual animals are plotted and colors are preserved for each animal throughout all panels. Using separate mixed-effects ANOVAs for each variable we measured, we sought to determine if the effects of lesions of M1 had differing effects across mice. We found that the rewarded trial rate did not vary as a function of mouse ($F(3,95) = 2.50$, $P = 0.06$) nor did the (B) average response time (log-transformed response time, $F(2,37) = 0.91$, $P = 0.41$), (C) the reach amplitude ($F(3,93) = 0.71$, $P = 0.59$), (D) the peak speed ($F(3,93) = 0.70$, $P = 0.56$), (D) the tortuosity ($F(3,93) = 1.29$, $P = 0.28$) or (F) the reach duration ($F(3,93) = 2.63$, $P = 0.06$). The mouse depicted by the dark purple performed 58 sessions prior to lesion. The mouse depicted by the light purple performed 19 sessions prior to lesion. The mouse depicted by green performed 39 sessions prior to lesion. The mouse depicted by maroon performed 52 sessions prior to lesion.

Supplemental Figure 3



Supplemental Figure 3. Striatal cell type identification and properties, related to Figures 3 and 4.

(A) Striatal cell identities were classified as spiny projection neurons, fast spiking interneurons, tonically active neurons or unidentified interneurons using a combination of proportion of long interspike-interval, post spike suppression and waveform duration. (B) Proportion of each cell type identified. Color legend is shared between panels A and B and C. (C) Example average waveform of identified neuron types (mean \pm SEM). (D) Cumulative histograms depicting no change in non task related Fano factor for SPNs (left) and FSIs (right). Colors for Pre and Post lesion epochs are conserved from the main text. To determine if lesions

of M1 affected non-task related neural activity, we calculated the Fano factor for each neuron. Spiking activity that occurred two seconds before and 5 seconds after a task related event (the cue light turning on or the start of a reach) was removed and then the remaining spike times were binned in non-overlapping 500 ms bins. For consistency across sessions, the first 100 seconds of this non-task related activity was used to obtain the Fano factor for each individual neuron. The mean Fano factor was calculated per session and each Post lesion epoch was compared to Pre using a two sampled t-test, corrected for multiple comparisons.

Supplemental Figure 4

A

SPN Reach Aligned Activity

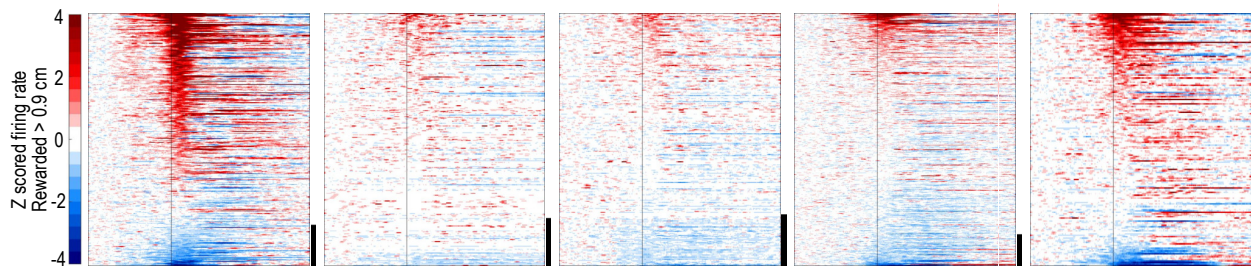
Pre

Post 1

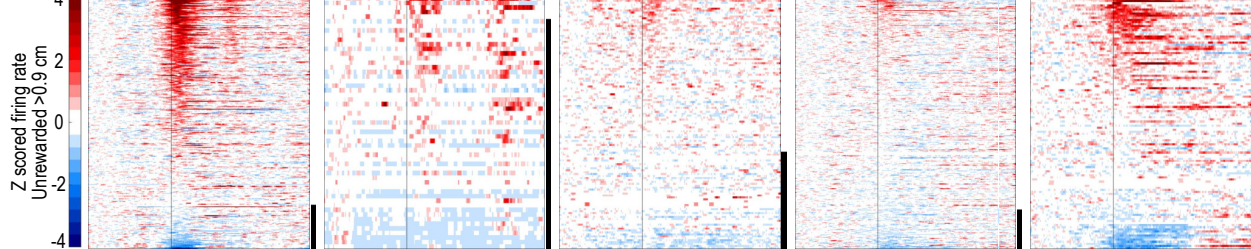
Post 2

Post 3

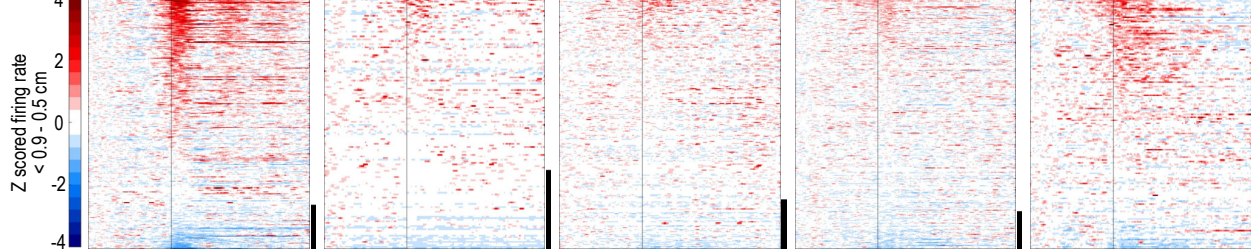
Post 4



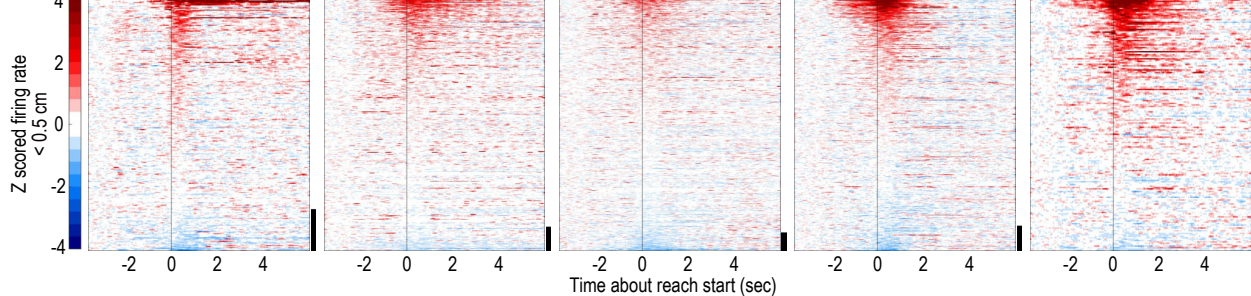
B



C



D

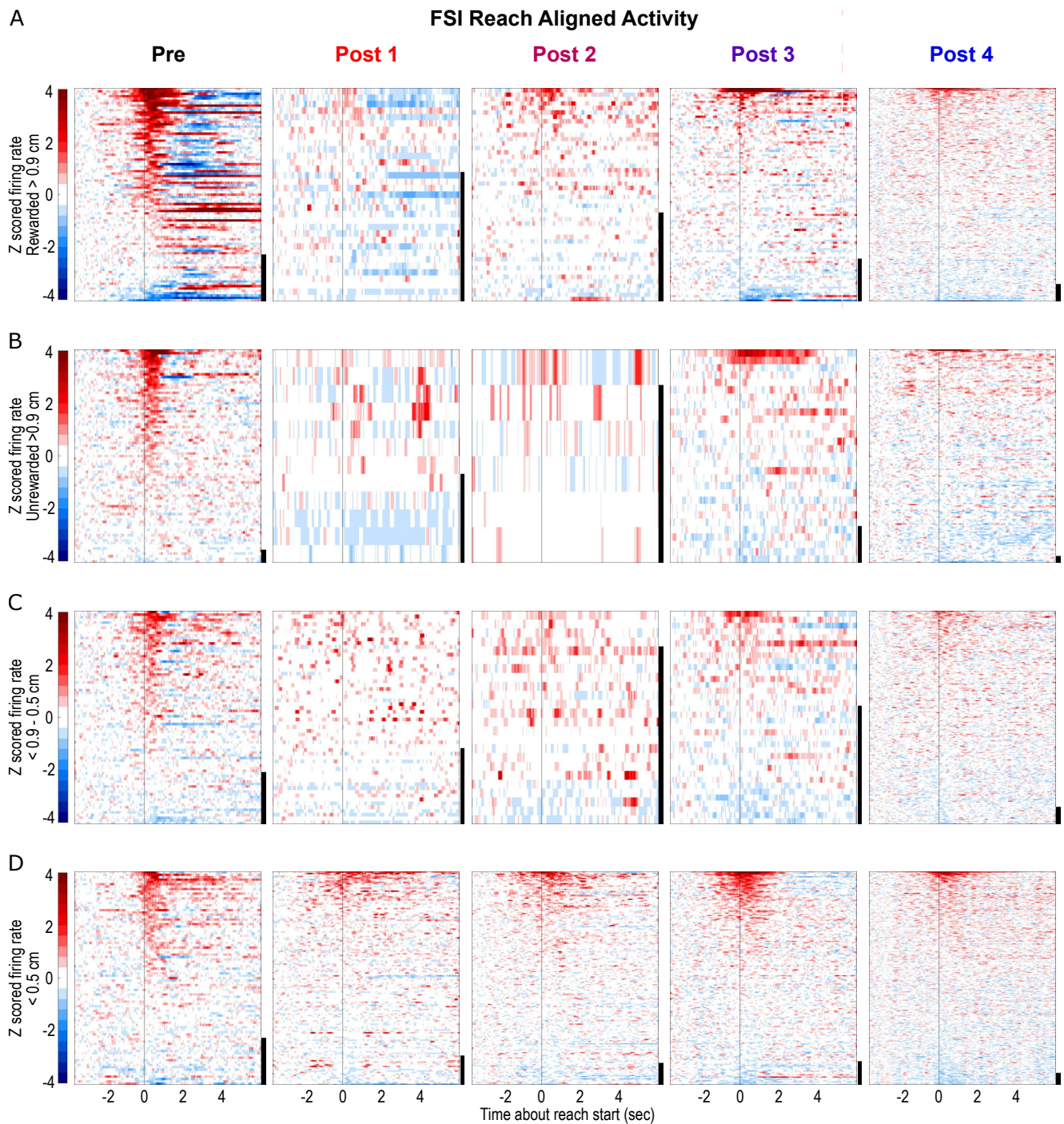


Supplemental Figure 4. Striatal SPN activity scales with reach amplitude and is lost post M1 lesions, related to Figure 3.

(A-D) Average Z-scored activity of putative SPNs from all sessions aligned to movement onset for rewarded

reaches (A), unrewarded reaches above the reward threshold (B), reaches below the reward threshold but above 0.5 cm (C) and reaches below 0.5 cm (D). The suprathreshold reaches that were unrewarded occurred during the ITI or reward delivery period. Neurons are sorted by their peak activity between -200 to 600 ms around movement onset. Y-scale bar indicates 50 neurons.

Supplemental Figure 5

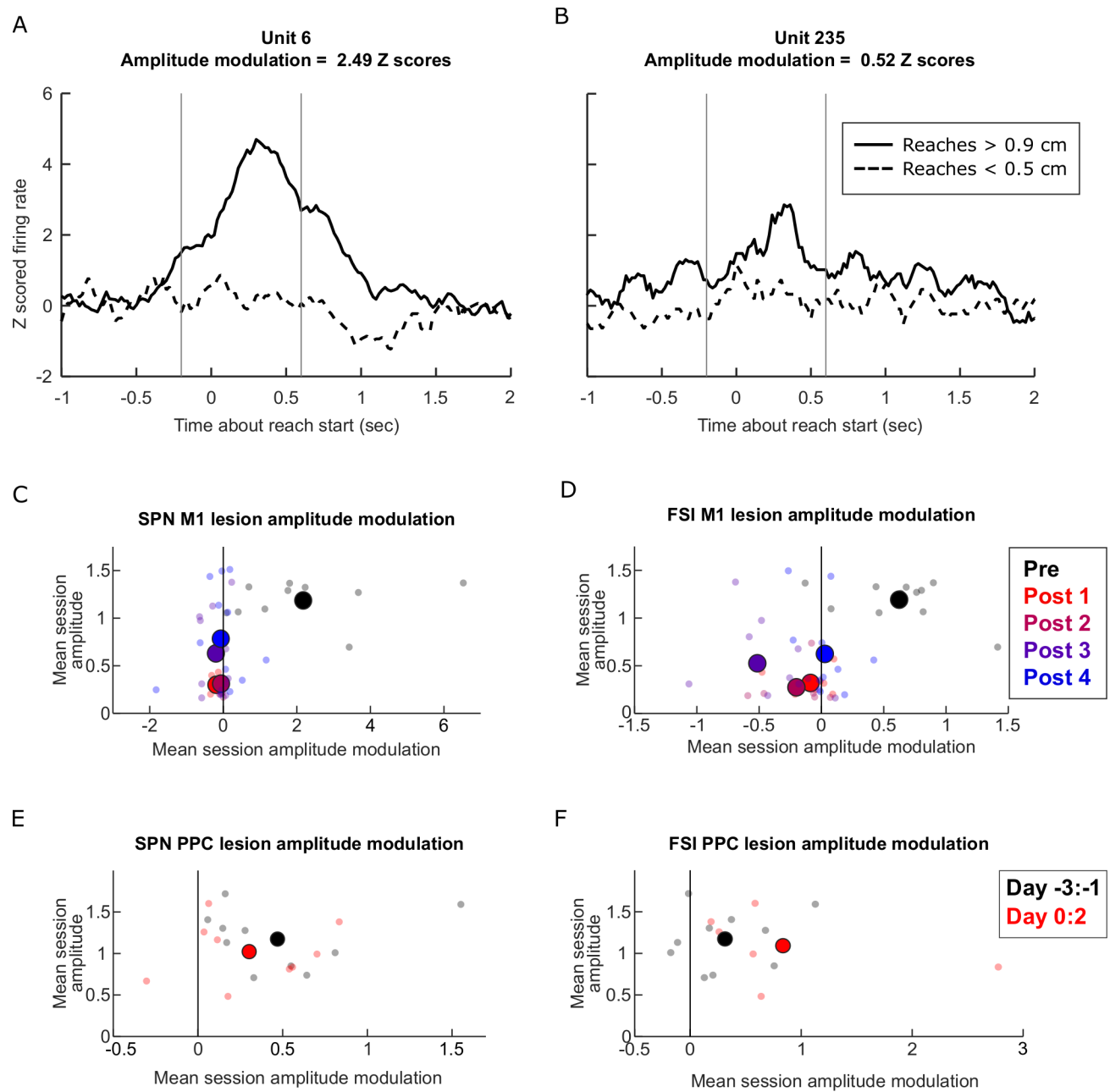


Supplemental Figure 5. Striatal FSI activity scales with reach amplitude and is lost post M1 lesions,

related to Figure 4.

(A-D) Average Z-scored activity of putative FSIs from all sessions aligned to movement onset for rewarded reaches (A), unrewarded reaches above the reward threshold (B), reaches below the reward threshold but above 0.5 cm (C) and reaches below 0.5 cm (D). The suprathreshold reaches that were unrewarded occurred during the ITI or reward delivery period. Neurons are sorted by their peak activity between -200 to 600 ms around movement onset. Y-scale bar indicates 20 neurons for all panels apart from panel B where the Y-scale bar indicates 5 neurons.

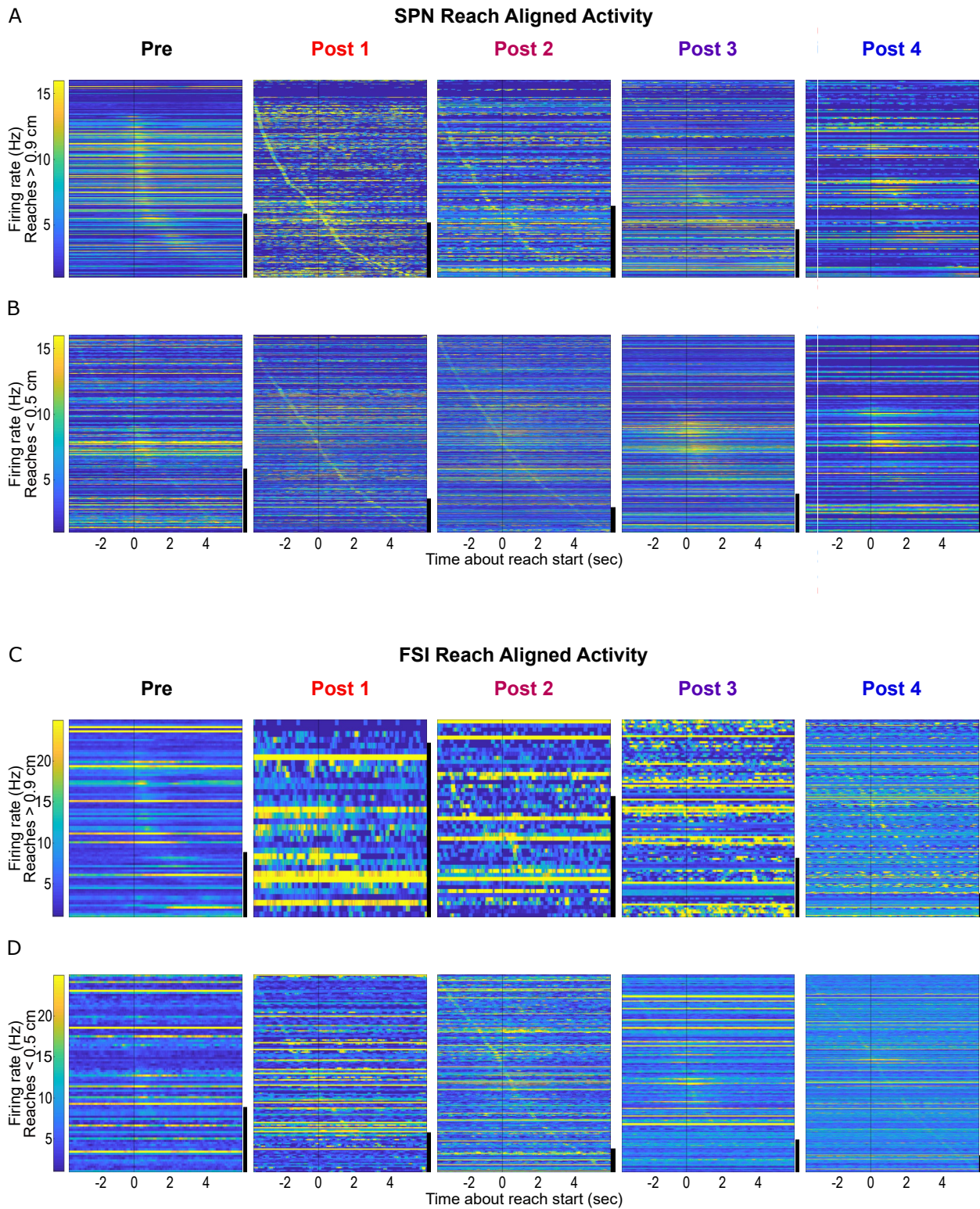
Supplemental Figure 6



Supplemental Figure 6. Amplitude modulation index example neurons and per session mean amplitude plotted against mean amplitude modulation - related to Figures 3, 4 and 6.

(A-B) Example putative SPN activity during reaches greater than 0.9 cm and reaches less than 0.5 cm recorded prior to lesions. The amplitude modulation index is calculated by taking the mean difference between the absolute Z scored activity during reaches greater than 0.9 cm and reached less than 0.5 cm between -200:600 ms around movement onset (vertical grey lines). (C-F) Comparison of mean amplitude modulation index and amplitude per session (small dots) for putative SPNs of M1 lesion mice (C), putative FSIs of M1 lesion mice (D), putative SPNs of PPC lesion mice (E) and putative FSIs for PPC lesion mice (F). Larger dots indicate post lesion epoch mean. Individual mixed-effects ANOVA models were run for each cell type and lesion group to determine if lesions affected amplitude modulation differently for different mice. For the M1 lesion group, we did find a main effect of mouse for amplitude modulate for SPNs ($F(2,45) = 11.58, P = 1.78 \times 10^{-4}$) however this was due to one animal. When the animal was removed from the ANOVA model we found no main effect of mouse ($F(1,35) = 2.98, P = 0.09$) while still finding a main effect of lesion ($F(2,35) = 8.92, P = 0.001$) suggesting that while one mouse is different, it is not the basis of our findings. We found no main effect of mouse for amplitude modulation for FSIs ($F(3,47) = 1.08, P = 0.37$). For the PPC lesion group, we found no main effect of mouse on amplitude modulation for SPNs ($F(1,18) = 0.22, P = 0.67$) nor FSIs ($F(2,15) = 2.36, P = 0.21$).

Supplemental Figure 7

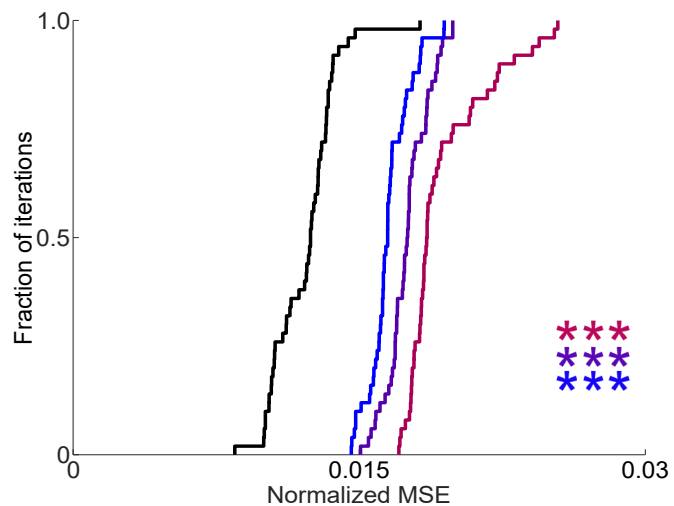


Supplemental Figure 7. Movement-related SPN and FSI activity is absent following bilateral M1 lesions - related to Figures 3 and 4.

(A-B) Raw firing rates of putative SPNs from all sessions aligned to movement onset for (A) reaches > 0.9 cm and (B) reaches < 0.5 cm. Neurons are sorted by their peak activity. Y-scale bar indicates 100 neurons.

(C-D) Activity of putative FSIs from all sessions aligned to movement onset for (C) reaches > 0.9 cm and (D) reaches < 0.5 cm. Neurons are sorted by their peak activity. Y-scale bar indicates 30 neurons. Neurons that did not respond during a particular reach type are not plotted. To help visualize tuning, neurons are rank ordered according to the time of peak activity. Vertical stacking of peak activity times, indicates a common temporal response profile across neurons. A diagonal 'line' indicates a random assortment of peak activity times.

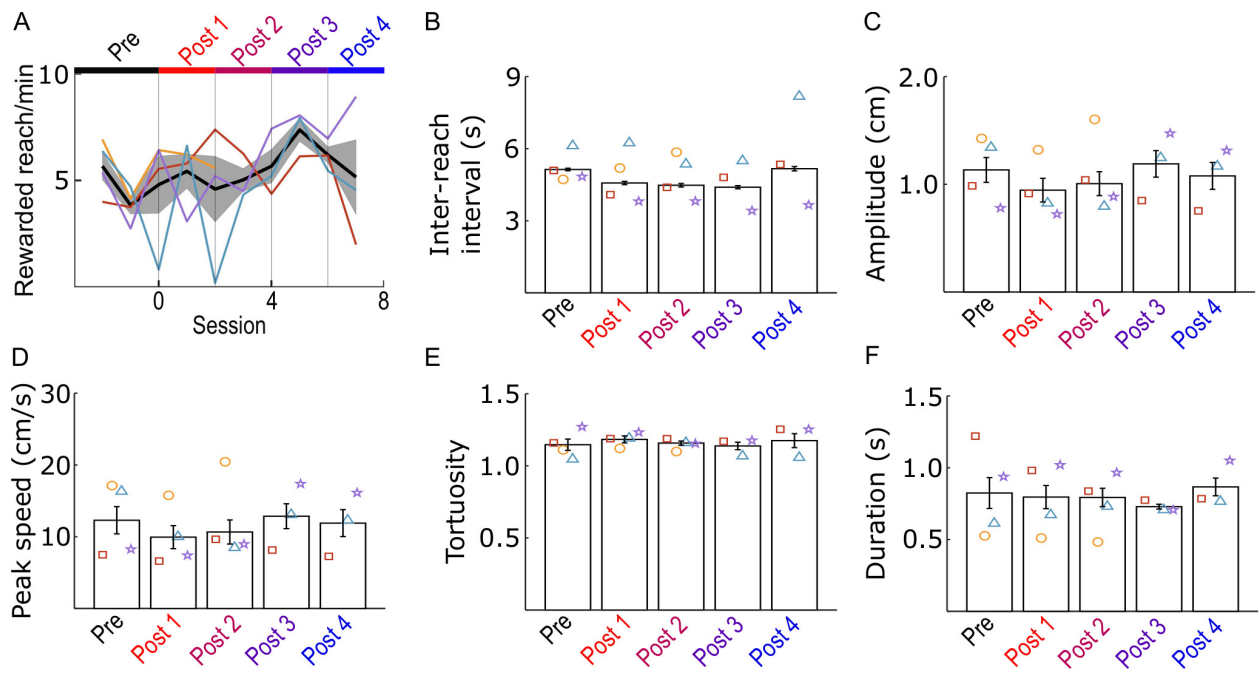
Supplemental Figure 8



Supplemental Figure 8. The ability to decoding joystick amplitude from striatal population activity is permanently lost following M1 lesions - related to Figure 5.

*Cumulative histogram of model performance across multiple iterations using a random subsample of reaches and neurons. Same as Figure 5B except with the use of 30 inputs instead of 10. *** = $p < 0.001$.*

Supplemental Figure 9

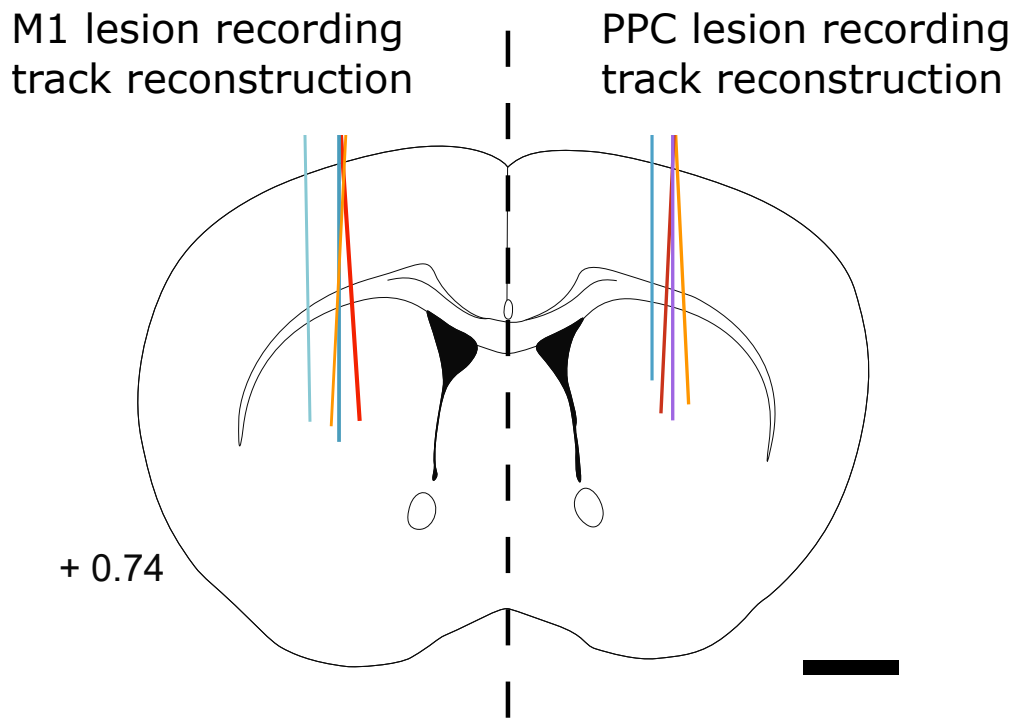


Supplemental Figure 9. Individual animal performance and kinematics during the basic reaching task, related to Figure 6.

(A) Mean rewarded reach rate over the first 20 minutes of each session relative to the day of lesion (mean \pm SEM) for mice run on the basic reaching task ($n = 4$). Colors for Pre and Post 1 through Post 4 are conserved across all subsequent figures. Individual animals are plotted and colors are preserved for each animal throughout all panels. To determine if lesions of PPC had differing effects of task performance and kinematics differently, we ran independent mixed-effects ANOVAs for each variable studied. We found no main effect of mouse for the rewarded trial rate ($F(3,34) = 0.35, P = 0.70$) nor for (B) reach amplitude ($F(3,34) = 0.74, P = 0.54$), or (C) reach speed ($F(3,34) = 0.96, P = 0.43$). We did find a main effect of mouse for (D) tortuosity ($F(3,39) = 3.30, P = 0.04$) and (F) reach duration ($F(3,34) = 4.55, P = 0.01$), however neither metric had a main effect of lesion (tortuosity, ($F(4,39) = 2.16, P = 0.10$), duration, $F(4,34) = 0.38, P = 0.82$). The mouse depicted by maroon performed 25 sessions prior to lesion. The mouse depicted by gold performed 44 sessions prior to lesion. The mouse depicted by light blue performed 64 sessions prior to lesion. The

mouse depicted by purple performed 73 sessions prior to lesion.

Supplemental Figure 10



Supplemental Figure 10. Reconstructed electrode tracks, related to Figures 3-6.

Approximate position of electrode from last recording sessions projected onto coronal atlas slice (plotted depicts the location and extent; see the Methods for actual electrode specifications). Left hemisphere depicts M1 lesioned mice. Right hemisphere depicts PPC lesioned mice, although all recordings were performed in the left hemisphere. Colors correspond to individual mouse colors used in previous per-animal plots. Scale bar = 1 mm.